INTERNATIONAL JOURNAL FOR NUMERICAL METHODS IN ENGINEERING
Int. J. Numer. Meth. Engng (in press)
Published online in Wiley InterScience (www.interscience.wiley.com). DOI: 10.1002/nme.1512

An energy-consistent material-point method for dynamic finite deformation plasticity

E. Love and D. L. Sulsky*, †

Department of Mathematics and Statistics, 415 Humanities Building, MSC03 2150, University of New Mexico, Albuquerque, NM 87131-0001, U.S.A.

SUMMARY

Energy consistency for the material-point method (MPM) is examined for thermodynamically consistent hyperelastic-plastic materials. It is shown that MPM can be formulated with implicit, three-field variational, finite element algorithms which dissipate energy and conserve momentum for that class of material models. With a consistent mass matrix the resulting overall numerical method inherits the energy-dissipative and momentum-conserving properties of the mesh solution. Thus, the proposed MPM algorithm satisfies by construction a time-discrete form of the second law of thermodynamics. Properties of the method are illustrated in numerical examples. Copyright © 2005 John Wiley & Sons, Ltd.

KEY WORDS: material-point method (MPM); energy consistency; momentum conservation; finite deformation plasticity

1. INTRODUCTION

The material-point method (MPM) is a general numerical tool for the mechanical analysis of continuous media [1–3]. This method utilizes two discretizations to solve the continuum equations describing the motion and deformation of fluids and solids. A Lagrangian description of the material under consideration is given by a set of unconnected material points that are tracked throughout the deformation. A background computational grid is used to calculate the interactions among the Lagrangian points through the solution of the momentum equation. A mapping between the two discretizations is performed at each step in the loading process. The constitutive equations are solved at each material point so that material models with history dependence are implemented easily. The method has proven to be particularly useful

*Correspondence to: D. L. Sulsky, Department of Mathematics and Statistics, 415 Humanities Building, MSC03 2150, University of New Mexico, Albuquerque, NM 87131-0001, U.S.A.
†E-mail: sulsky@math.unm.edu

Contract/grant sponsor: National Science Foundation; contract/grant number: DMS-0222253

Received 19 January 2005
Revised 4 April 2005
Accepted 18 July 2005

for problems displaying the large deformation that occurs with inelastic behaviour of solids. The present work exploits developments in finite element analysis to construct an implicit energy and momentum consistent method for hyperelastic-plastic solids.

This effort extends the work of References [4–6]. For typical deviatoric metal plasticity the possible locking of a finite element (or MPM) approximation becomes an important consideration. Most research to date in MPM has not directly addressed this issue. In the present paper, in an effort to avoid an overconstrained pressure approximation, a three-field mixed formulation is considered. In principle, this formulation not only avoids volumetric locking but also provides for a more general implementation than the two-field mixed (MPM) formulation in Reference [7]. Additionally, this paper examines the energy consistency of the MPM numerical algorithm for non-linear hyperelastic-plastic models, which has not been addressed previously.

Section 2 of this paper presents the continuum equations and reviews their conservation properties. The goal is to replicate these continuum properties in the discrete equations. Section 3 reviews the MPM computational cycle, including the integration of the plasticity equations, and examines conservation properties of the discretization. In order to have an energy-consistent method, the Lagrangian grid dynamics must dissipate energy and conserve momentum. For this step we make use of an implicit time integration scheme developed for the finite element method which has the desired properties. Thus, analysis of the grid dynamics follows [8, 9]. The MPM algorithm inherits the properties of the grid dynamics algorithm if a consistent mass matrix is used [5, 10].

Finally, in Section 4, numerical examples are presented that illustrate the properties of this energy-consistent and momentum-conserving MPM. Section 5 concludes the paper with some remarks and observations.

2. THE CONTINUUM PROBLEM

The goal of this section is to present the continuum equations of motion for a deformable solid body. These equations are well known, and the reader may consult the books [11–14] or [15] for more information. After introducing the notation, the weak form of the linear momentum equation and the hyperelastic-plastic constitutive model are given. A three-field mixed variational principle, presented in this section, forms the basis for the numerical discretization of the subsequent sections. Finally, conservation of linear momentum, angular momentum and energy are reviewed for the unforced, traction-free Neumann problem. The discrete equations should ideally have similar conservation properties.

2.1. Basic notation

Let $\Omega_0 \in \mathbb{R}^3$ denote the reference (material) position of a continuum body, with material points labelled $\mathbf{X}$. The set Ω_0 is assumed open and bounded, with a smooth boundary Γ_0. Assume the reference boundary Γ_0 is partitioned into disjoint subsets such that $\Gamma_0 = \overline{\Gamma_{\boldsymbol{\varphi}} \bigcup \Gamma_{\boldsymbol{\sigma}}}$ and $\Gamma_{\boldsymbol{\varphi}} \bigcap \Gamma_{\boldsymbol{\sigma}} = \emptyset$.

Let the spatial (current) position of the same body be $\Omega \in \mathbb{R}^3$, with points labelled $\mathbf{x}$. Assume there exists a smooth mapping, the motion of the body, $\boldsymbol{\varphi} : \Omega_0 \times [0, T] \to \mathbb{R}^3$, such that $\Omega = \boldsymbol{\varphi}(\Omega_0, t)$ and $\mathbf{x} = \boldsymbol{\varphi}(\mathbf{X}, t)$, where $[0, T] \subset \mathbb{R}$ is the time interval of interest. The deformation gradient of the motion is defined as

$$\mathbf{F}(\mathbf{X}, t) := D\boldsymbol{\varphi} = \mathrm{GRAD}_{\mathbf{X}}[\boldsymbol{\varphi}] \tag{1}$$

Given the above, the set of admissible configurations is then defined as

$$\mathscr{S} := \{\boldsymbol{\varphi} : \Omega_0 \times [0, T] \to \mathbb{R}^3 \mid J(\boldsymbol{\varphi}) := \det[\mathbf{F}] > 0 \text{ and } \boldsymbol{\varphi}|_{\Gamma_{\boldsymbol{\varphi}}} = \bar{\boldsymbol{\varphi}}\} \tag{2}$$

where $\bar{\boldsymbol{\varphi}} : \Gamma_{\boldsymbol{\varphi}} \times [0, T] \to \mathbb{R}^3$ is specified on $\Gamma_{\boldsymbol{\varphi}}$. The material velocity of a point $\mathbf{X}$ is defined as $\mathbf{v} := \dot{\boldsymbol{\varphi}}$, where the superposed dot denotes the material time derivative. Given a reference density $\rho_0 : \Omega_0 \to \mathbb{R}^+$, the spatial density is $\rho = J^{-1}\rho_0$ and the material momentum is defined as $\boldsymbol{\pi} := \rho_0 \mathbf{v}$.

Let $\boldsymbol{\sigma}$ denote the Cauchy stress in the current configuration. The developments in this work critically use the *symmetric* Piola–Kirchhoff stress $\mathbf{S}$, defined such that

$$J\boldsymbol{\sigma} = \mathbf{F}\mathbf{S}\mathbf{F}^{\mathrm{T}} \tag{3}$$

The Kirchhoff stress is defined as

$$\boldsymbol{\tau} := \boldsymbol{\varphi}_*(\mathbf{S}) = \mathbf{F}\mathbf{S}\mathbf{F}^{\mathrm{T}} \tag{4}$$

with *deviatoric part* $\operatorname{dev}\boldsymbol{\tau} := \boldsymbol{\tau} - \frac{1}{3}\operatorname{trace}[\boldsymbol{\tau}]\mathbf{I}$, where $\boldsymbol{\varphi}_*(\cdot)$ denotes the standard push-forward operation [14, 16] of continuum mechanics and differential geometry, with corresponding pull back operation denoted by $\boldsymbol{\varphi}^*(\cdot)$. The prescribed traction boundary condition is

$$(\mathbf{F}\mathbf{S})\mathbf{N} = \bar{\mathbf{T}} \quad \text{on } \Gamma_{\boldsymbol{\sigma}} \tag{5}$$

where $\mathbf{N} : \Gamma_0 \to S^2$ is the outward unit normal field to the material boundary Γ_0 and $\bar{\mathbf{T}} : \Gamma_{\boldsymbol{\sigma}} \times [0, T] \to \mathbb{R}^3$ is the prescribed nominal traction vector. In addition to these boundary tractions, the body is assumed to be acted upon by a body force (per unit mass) $\mathbf{g} : \Omega_0 \times [0, T] \to \mathbb{R}^3$.

2.2. Three-field variational principle

As stated in the introduction, a three-field mixed variational principle is to be considered. The principle essentially involves a volumetric–deviatoric split of the governing equations in order to introduce separate interpolations for volumetric deformation and pressure. If properly chosen, these additional interpolated fields should alleviate the locking phenomena typically observed in standard, non-mixed finite element approximations. The three-field principle is most easily presented within the context of elasticity, and may be subsequently applied to plasticity as an extension.

Denote by $\mathscr{T}_{3\times3}$ the space of all rank two tensors. Let $\mathscr{T}^{\mathrm{sym}}_{3\times3}$ be the subspace of all symmetric rank two tensors and $\mathscr{T}^{\mathrm{sym}+}_{3\times3}$ be the convex subset of all symmetric, positive-definite rank two tensors. Let $\mathbf{C} := \mathbf{F}^{\mathrm{T}}\mathbf{F}$ denote the right Cauchy–Green strain tensor and $\mathbf{b} := \mathbf{F}\mathbf{F}^{\mathrm{T}}$ denote the left Cauchy–Green strain tensor. Note that $\mathbf{C}$ and $\mathbf{b}$ have the same invariants and eigenvalues.

Initially, we shall assume that the body is isotropic and hyperelastic, so that at each material point $\mathbf{X} \in \Omega_0$ there exists an internal free energy of the form

$$W(\mathbf{C}) := \hat{W}(\mathbf{C}) + U(\det(\mathbf{C})^{1/2}) \tag{6}$$

where $\hat{W}$ is the deviatoric energy,

$$\hat{W}(\lambda\mathbf{C}) = \hat{W}(\mathbf{C}) \quad \forall \mathbf{C} \in \mathscr{T}^{\mathrm{sym}+}_{3\times3} \quad \text{and} \quad \forall \lambda \in \mathbb{R}^+ \tag{7}$$

and $U(J)$ is the volumetric energy. Under the assumption of isotropy, the energy function $\hat{W}$ is a function only of the invariants of $\mathbf{C}$ (see the appendix of Reference [13]), or equivalently only of the invariants of $\mathbf{b}$. Thus, there exists a $\tilde{W}(\mathbf{b})$ such that $\hat{W}(\mathbf{C}) = \tilde{W}(\mathbf{b})$, where isotropy (and invariance under superposed rigid body motions) requires that

$$\tilde{W}(\mathbf{Q}\mathbf{b}\mathbf{Q}^{\mathrm{T}}) = \tilde{W}(\mathbf{b}) \quad \forall \mathbf{Q} \in SO(3) \tag{8}$$

Given isotropy, Equation (6) may be written equivalently as a function of $\mathbf{b}$, so that

$$W(\mathbf{b}) := \tilde{W}(\mathbf{b}) + U(\det(\mathbf{b})^{1/2}) \tag{9}$$

Denote by $\mathscr{W}$ the space of test functions associated with the admissible configurations in $\mathscr{S}$, defined in standard fashion as

$$\mathscr{W} := \{\delta\boldsymbol{\varphi} : \Omega_0 \to \mathbb{R}^3 \mid \delta\boldsymbol{\varphi}|_{\Gamma_{\boldsymbol{\varphi}}} = \mathbf{0}\} \tag{10}$$

It is convenient to introduce two inner product notations, $\langle \cdot, \cdot \rangle_{\Omega_0}$ and $\langle \cdot, \cdot \rangle_{\Gamma_0}$, denoting the L^2 inner product on Ω_0 and Γ_0, respectively, of scalars, vectors or tensors, depending on the context.

A three-field variational statement [17, 18] of the equations of motion for a solid body can be derived from a Lagrangian of the form

$$\mathrm{L}(\boldsymbol{\varphi}, \mathbf{v}, \Theta, p) = \frac{1}{2}\langle \mathbf{v}, \rho_0 \mathbf{v} \rangle_{\Omega_0} - \int_{\Omega_0} [\hat{W}(\mathbf{C}) + p(J(\mathbf{C}) - \Theta) + U(\Theta)]\, \mathrm{d}\Omega_0 - \Pi_{\mathrm{ext}}(\boldsymbol{\varphi}) \tag{11}$$

for $\boldsymbol{\varphi} \in \mathscr{S}$, $\mathbf{v} \in \mathscr{W}$ and $p, \Theta \in L^2(\Omega_0)$. The variables $\{p, \Theta\}$ are the mixed pressure and the mixed volume, respectively. The external force potential function is

$$\Pi_{\mathrm{ext}}(\boldsymbol{\varphi}) = \int_{\Omega_0} \pi_g(\boldsymbol{\varphi})\, \mathrm{d}\Omega_0 + \int_{\Gamma_0} \pi_T(\boldsymbol{\varphi})\, \mathrm{d}\Gamma_0 \tag{12}$$

with the additional definitions $\mathbf{g} := -\partial_{\boldsymbol{\varphi}} \pi_g$ and $\bar{\mathbf{T}} := -\partial_{\boldsymbol{\varphi}} \pi_T$.

The Euler–Lagrange equations associated with this Lagrangian are: find $\boldsymbol{\varphi} \in \mathscr{S}$ and p, $\Theta \in L^2(\Omega_0)$ such that

$$\langle \delta\boldsymbol{\varphi}, \dot{\boldsymbol{\pi}} \rangle_{\Omega_0} + \langle \mathrm{GRAD}_{\mathbf{X}}[\delta\boldsymbol{\varphi}], \mathbf{FS} \rangle_{\Omega_0} - \langle \delta\boldsymbol{\varphi}, \rho_0 \mathbf{g} \rangle_{\Omega_0} - \langle \delta\boldsymbol{\varphi}, \bar{\mathbf{T}} \rangle_{\Gamma_0} = 0 \tag{13a}$$

$$\langle \delta\Theta, p - \partial_{\Theta} U \rangle_{\Omega_0} = 0 \tag{13b}$$

$$\langle \delta p, J(\mathbf{C}) - \Theta \rangle_{\Omega_0} = 0 \tag{13c}$$

for all $\delta\boldsymbol{\varphi} \in \mathscr{W}$ and for all $\delta p, \delta\Theta \in L^2(\Omega_0)$, where

$$\begin{aligned} \mathbf{S} &= 2\partial_{\mathbf{C}} \hat{W} + 2p(\partial_{\mathbf{C}} J) \\ &= \boldsymbol{\varphi}^*(\mathrm{dev}\, \boldsymbol{\tau} + pJ\mathbf{I}) \end{aligned} \tag{14}$$

and $2\partial_{\mathbf{C}} J = J\mathbf{C}^{-1}$.

Along with the above variational equation, the solution $\boldsymbol{\varphi}$ must also satisfy the initial conditions

$$\boldsymbol{\varphi}(\mathbf{X}, 0) = \boldsymbol{\varphi}_0 \quad \text{and} \quad \boldsymbol{\pi}(\mathbf{X}, 0) = \rho_0 \mathbf{v}_0 \quad \text{in } \Omega_0 \tag{15}$$

Once a suitable constitutive equation relating $\mathbf{S}$ to the motion $\boldsymbol{\varphi}$ is specified, Equations (13) and (15) together define a (generally) non-linear initial boundary value problem for the motion $\boldsymbol{\varphi} \in \mathscr{S}$ of the body.

Remark 2.1

1. As previously mentioned, although Equations (13) have been derived as the Euler–Lagrange equations of a Lagrangian potential function, they are more generally applicable to non-conservative and dissipative dynamical processes. In this work they are used in the numerical simulation of plasticity.
2. The Lagrangian (11) is actually a simplified version of the more general Lagrangian

$$\mathrm{L}(\boldsymbol{\varphi}, \mathbf{v}, \Theta, p) = \frac{1}{2}\langle \mathbf{v}, \rho_0 \mathbf{v} \rangle_{\Omega_0} - \int_{\Omega_0} \{W((\Theta/J)^{1/3}\mathbf{C}) + p(J - \Theta)\}\, \mathrm{d}\Omega_0 - \Pi_{\mathrm{ext}}(\boldsymbol{\varphi})$$

   where no *a priori* assumptions about the character of the free energy W are made [8, 17–19]. However, under the conditions of Equation (6), this more general expression collapses to the form in (11), which is both simpler to implement and sufficient for the purposes of this work.
3. An augmented Lagrangian algorithm [8, 17, 20] can be applied within this three-field mixed framework to enforce the incompressibility constraint $\Theta = 1$. Reference [7] considers a two-field $\{\boldsymbol{\varphi}, p\}$ formulation for incompressibility within an MPM context.

2.3. Isotropic multiplicative plasticity

The goal is the numerical simulation of dynamic finite deformation plasticity. Without any significant loss of generality, attention is restricted to the isotropic case.

2.3.1. Basic assumptions. Isotropic finite strain multiplicative plasticity with isotropic hardening has the following set of assumptions [21–23]:

1. There exists a convex elastic domain

$$\mathbb{E} := \{(\boldsymbol{\tau}, q) \in \mathscr{T}^{\mathrm{sym}}_{3\times 3} \times \mathbb{R} \mid \Phi(\boldsymbol{\tau}, q) \leqslant 0\} \tag{16}$$

   with boundary $\partial\mathbb{E}$, where q is a scalar stress-like isotropic hardening variable and Φ is the (smooth) yield function. Invariance under superposed rigid body motions requires Φ to be an isotropic function of the stress,

$$\Phi(\mathbf{Q}\boldsymbol{\tau}\mathbf{Q}^{\mathrm{T}}, q) = \Phi(\boldsymbol{\tau}, q) \quad \forall \mathbf{Q} \in SO(3) \tag{17}$$

2. The deformation gradient admits a multiplicative decomposition into elastic and plastic parts [24, 25] such that

$$\mathbf{F} = \mathbf{F}^{\mathrm{e}}\mathbf{F}^{\mathrm{p}} \tag{18}$$

Consistent with this define $J^{\mathrm{e}} := \det \mathbf{F}^{\mathrm{e}}$ and $J^{\mathrm{p}} := \det \mathbf{F}^{\mathrm{p}}$ so that $J = J^{\mathrm{e}} J^{\mathrm{p}}$. All developments herein are based upon the elastic left Cauchy–Green strain tensor

$$\mathbf{b}^{\mathrm{e}} := \mathbf{F}^{\mathrm{e}} \mathbf{F}^{\mathrm{e}\mathrm{T}} \tag{19}$$

and the inverse plastic metric

$$\mathbf{G}^{\mathrm{p}} := [\mathbf{F}^{\mathrm{p}\mathrm{T}} \mathbf{F}^{\mathrm{p}}]^{-1} \tag{20}$$

where

$$\mathbf{b}^{\mathrm{e}} = \mathbf{F} \mathbf{G}^{\mathrm{p}} \mathbf{F}^{\mathrm{T}} \tag{21}$$

3. The stress response of the material is given by an internal free energy function $W(\mathbf{b}^{\mathrm{e}}, \xi)$, where $\xi \geqslant 0$ is a scalar strain-like isotropic hardening variable. The stress-like hardening variable q is conjugate to ξ in the sense that

$$q := -\partial_{\xi} W \tag{22}$$

Invariance requires that the free energy function W be isotropic in the sense that

$$W(\mathbf{Q} \mathbf{b}^{\mathrm{e}} \mathbf{Q}^{\mathrm{T}}, \xi) = W(\mathbf{b}^{\mathrm{e}}, \xi) \quad \forall \mathbf{Q} \in SO(3) \tag{23}$$

2.3.2. Dissipation inequality. Given the assumptions of Section 2.3.1, it is necessary to derive thermodynamically consistent constitutive equations for the elastic response of the material and the evolution of the plastic internal variables. The starting point for the derivation is a reduced form of the second law of thermodynamics. At every material point $\mathbf{X} \in \Omega_0$ the internal dissipation rate is defined as

$$\begin{aligned} \mathscr{D}^{\mathrm{int}} &:= \boldsymbol{\tau} : \mathbf{d} - \frac{\mathrm{d}}{\mathrm{d}t} W(\mathbf{b}^{\mathrm{e}}, \xi) \geqslant 0 \\ &= \frac{1}{2} \mathbf{S} : \dot{\mathbf{C}} - \frac{\mathrm{d}}{\mathrm{d}t} W(\mathbf{b}^{\mathrm{e}}, \xi) \geqslant 0 \end{aligned} \tag{24}$$

where the rate of deformation tensor is $\mathbf{d} = \mathrm{sym}(\mathbf{l}) = \mathrm{sym}(\dot{\mathbf{F}} \mathbf{F}^{-1}) = \frac{1}{2} \boldsymbol{\varphi}_*(\dot{\mathbf{C}})$. Equation (24) and a standard sequence of thermodynamic arguments [11, 21–23] yield the elastic response

$$\boldsymbol{\tau} = 2 \mathbf{b}^{\mathrm{e}} (\partial_{\mathbf{b}^{\mathrm{e}}} W) = 2 (\partial_{\mathbf{b}^{\mathrm{e}}} W) \mathbf{b}^{\mathrm{e}} \tag{25}$$

and a remaining dissipation inequality

$$\mathscr{D}^{\mathrm{int}} = \boldsymbol{\tau} : [-\tfrac{1}{2} (\mathscr{L}_v \mathbf{b}^{\mathrm{e}}) \mathbf{b}^{\mathrm{e}-1}] + q \dot{\xi} \geqslant 0 \tag{26}$$

where

$$\mathscr{L}_v \mathbf{b}^{\mathrm{e}} := \mathbf{F} \left[\frac{\mathrm{d}}{\mathrm{d}t} \mathbf{G}^{\mathrm{p}} \right] \mathbf{F}^{\mathrm{T}} \tag{27}$$

is the Lie derivative of $\mathbf{b}^{\mathrm{e}}$. The adoption of *associative* flow rules for the internal plastic parameters results in

$$-\tfrac{1}{2}(\mathscr{L}_v \mathbf{b}^{\mathrm{e}}) = \dot{\gamma}[\partial_{\boldsymbol{\tau}}\Phi]\mathbf{b}^{\mathrm{e}} \tag{28a}$$

$$\dot{\xi} = \dot{\gamma}\partial_q \Phi \tag{28b}$$

for a plastic consistency parameter $\dot{\gamma} \geqslant 0$. This reduces the internal dissipation rate to

$$\mathscr{D}^{\mathrm{int}} = \dot{\gamma}[(\boldsymbol{\tau} : \partial_{\boldsymbol{\tau}}\Phi) + (q \cdot \partial_q \Phi)] \geqslant 0 \tag{29}$$

Using Equations (21) and (27) the flow rule (28a) has the equivalent form

$$\dot{\mathbf{G}}^{\mathrm{p}} = -2\dot{\gamma}(\mathbf{F}^{-1}[\partial_{\boldsymbol{\tau}}\Phi]\mathbf{F})\mathbf{G}^{\mathrm{p}} \tag{30}$$

The plastic consistency parameter $\dot{\gamma} \geqslant 0$ remains to be defined. There are two cases of interest.

1. *Rate-independent plasticity*. In this case $\dot{\gamma}$ is the Lagrange multiplier associated with the inequality constraint $\Phi \leqslant 0$ and is given by the Kuhn–Tucker conditions

$$\dot{\gamma} \geqslant 0, \quad \Phi \leqslant 0, \quad \dot{\gamma}\Phi = 0 \tag{31}$$

2. *Viscoplasticity*. In this case $\dot{\gamma}$ is given by a viscoplastic regularization

$$\dot{\gamma} = \frac{\langle \Phi \rangle}{\eta} \tag{32}$$

where $\eta > 0$ is the viscosity parameter. The Macauley bracket function is

$$\langle x \rangle = \tfrac{1}{2}(x + |x|) \tag{33}$$

In the limit as $\eta \searrow 0$ the rate-independent case is recovered.

Since the elastic domain $\mathbb{E} \subset \mathbb{R}^7$ is a convex set containing the origin, the inequality $[(\boldsymbol{\tau} : \partial_{\boldsymbol{\tau}}\Phi) + (q \cdot \partial_q \Phi)] \geqslant 0 \forall (\boldsymbol{\tau}, q) \in \partial\mathbb{E}$ holds, and the dissipation inequality (29) is satisfied by construction.

2.3.3. J^2 flow model. For the purposes of this work, a J^2 flow model of plasticity is considered in the numerical examples. The model is as follows:

- The yield function takes the simple form

$$\Phi(\boldsymbol{\tau}, q) := \|\mathrm{dev}\,\boldsymbol{\tau}\| - \sqrt{\tfrac{2}{3}}(\sigma_Y - q) \tag{34}$$

where $\sigma_Y \geqslant 0$ is the flow (yield) stress. In this case

$$\mathbf{n} := \partial_{\boldsymbol{\tau}}\Phi = \frac{\mathrm{dev}\,\boldsymbol{\tau}}{\|\mathrm{dev}\,\boldsymbol{\tau}\|} \tag{35}$$

and

$$\partial_q \Phi = \sqrt{\tfrac{2}{3}} \tag{36}$$

so that

$$\dot{\mathbf{G}}^{\mathrm{p}} = -2\dot{\gamma}(\mathbf{F}^{-1}\mathbf{n}\,\mathbf{F})\mathbf{G}^{\mathrm{p}} \tag{37}$$

and

$$\dot{\xi} = \dot{\gamma}\sqrt{\tfrac{2}{3}} \tag{38}$$

The internal dissipation rate (29) simplifies to

$$\begin{aligned}\mathscr{D}^{\mathrm{int}} &= \dot{\gamma}\left[\|\mathrm{dev}\,\boldsymbol{\tau}\| + q\sqrt{\tfrac{2}{3}}\right] \\ &= \dot{\gamma}\left[\Phi + \sqrt{\tfrac{2}{3}}(\sigma_Y - q) + q\sqrt{\tfrac{2}{3}}\right] \\ &= \dot{\gamma}\left[\Phi + \sqrt{\tfrac{2}{3}}\sigma_Y\right]\end{aligned} \tag{39}$$

For this classical model of plasticity, the hardening parameter ξ is often termed the *equivalent plastic strain*.

- Let $\boldsymbol{\varepsilon}^{\mathrm{e}} = \mathrm{diag}\{\varepsilon_1^{\mathrm{e}}, \varepsilon_2^{\mathrm{e}}, \varepsilon_3^{\mathrm{e}}\}$ be the vector of principal logarithmic elastic stretches, the log of the eigenvalues of $\sqrt{\mathbf{b}^{\mathrm{e}}}$. Let $\boldsymbol{\beta} = \mathrm{diag}\{\beta_1, \beta_2, \beta_3\}$ be the vector of principal Kirchhoff stresses, the eigenvalues of $\boldsymbol{\tau}$. For isotropic models one can use the chain rule to show that $\beta_A = \partial_{\varepsilon_A^{\mathrm{e}}} W$ [26]. The elastic response is given by

$$W(\mathbf{b}^{\mathrm{e}}, \xi) = G\|\mathrm{dev}\,\boldsymbol{\varepsilon}^{\mathrm{e}}\|^2 + U(J^{\mathrm{e}}) + \mathscr{H}(\xi) \tag{40}$$

where $G \geqslant 0$ is the (linearized) elastic shear modulus. This is often referred to as the Hencky model of finite strain elasticity [22, 26]. Note that this free energy function satisfies the assumption of Equations (6) and (9) so that

$$\tilde{W}(\mathbf{b}^{\mathrm{e}}, \xi) = G\|\mathrm{dev}\,\boldsymbol{\varepsilon}^{\mathrm{e}}\|^2 + \mathscr{H}(\xi) \implies \mathrm{dev}\,\boldsymbol{\tau} = 2(\partial_{\mathbf{b}^{\mathrm{e}}}\tilde{W})\mathbf{b}^{\mathrm{e}} \tag{41}$$

For the Hencky model the principal values of dev $\boldsymbol{\tau}$ are $\boldsymbol{\beta} = \partial_{\boldsymbol{\epsilon}^{\mathrm{e}}}\tilde{W} = 2G\,\mathrm{dev}\,\boldsymbol{\epsilon}^{\mathrm{e}}$. Finally, for linear isotropic hardening

$$\mathscr{H}(\xi) := \tfrac{1}{2}H\xi^2 \tag{42}$$

with the hardening parameter $H \geqslant 0$, so that $q = -H\xi$.

Remark 2.2

1. Unfortunately, the Hencky model of finite strain elasticity is not polyconvex [21, 22]. Thus, it is not appropriate for use when large elastic strains are present, and in fact numerical difficulties have been encountered [27]. However, the model very much simplifies the numerical implementation of the plasticity equations and provides a valid approximation for small to moderate elastic strains. For typical metal plasticity the elastic strains are small relative to the plastic strains, and the Hencky model is suitable.

2. It is not strictly necessary to assume that the yield function is based upon the Kirchhoff stresses $\boldsymbol{\tau}$. The equations can be formulated assuming that the Cauchy stresses $\boldsymbol{\sigma}$ determine the yield criterion, and one might argue this to be more physically correct. In such a situation the flow rules are by necessity non-associative, even with the postulate of maximum plastic dissipation [28]. For this presentation it is sufficient to consider the plasticity equations as presented above, with the knowledge that a modification to the constitutive model is not difficult.

2.4. Conservation properties

In this section, linear momentum, angular momentum, and total energy, are defined, and the fact that the dynamical system governed by (13) conserves momentum and dissipates total energy under appropriate loading and boundary conditions, is recalled. When an MPM numerical approximation of the equations of motion is introduced, said approximation shall be constructed so as to reproduce these conservation properties of the continuum problem.

Definition 2.1
The *total linear momentum* $\mathbf{L}$ is defined as

$$\mathbf{L} := \int_{\Omega_0} \boldsymbol{\pi} \, \mathrm{d}\Omega_0 \tag{43}$$

Definition 2.2
The *total angular momentum* $\mathbf{J}$ is defined as

$$\mathbf{J} := \int_{\Omega_0} (\boldsymbol{\varphi} \times \boldsymbol{\pi}) \, \mathrm{d}\Omega_0 \tag{44}$$

Definition 2.3
The *total kinetic energy* T is defined as

$$2\mathsf{T} := \langle \boldsymbol{\pi}, \rho_0^{-1} \boldsymbol{\pi} \rangle_{\Omega_0} = \langle \boldsymbol{\pi}, \mathbf{v} \rangle_{\Omega_0} = \langle \rho_0 \mathbf{v}, \mathbf{v} \rangle_{\Omega_0} \tag{45}$$

Definition 2.4
The *total potential energy* V is defined as

$$\mathsf{V} := \int_{\Omega_0} [\tilde{W}(\mathbf{b}^{\mathrm{e}}, \xi) + U(\Theta)] \, \mathrm{d}\Omega_0 \tag{46}$$

Definition 2.5
The *total energy* H is defined as

$$\mathsf{H} := \mathsf{T} + \mathsf{V} \tag{47}$$

Theorem 2.1
Let $\Gamma_{\boldsymbol{\varphi}} = \emptyset$, $\mathbf{b} = \mathbf{0}$ and $\bar{\mathbf{T}} = \mathbf{0}$. Then total linear momentum $\mathbf{L}$ and the total angular momentum $\mathbf{J}$ are constants of the motion, and the total energy H is dissipated.

Proof
This result is well known, and is based on classical arguments.

1. *Linear momentum is conserved*. See References [8, 29].
2. *Angular momentum is conserved*. Conservation of angular momentum is a direct result of the symmetry of the stress tensor $\mathbf{S}$ [8, 29].
3. *Energy is dissipated*. Consider variations of the form

$$\delta\boldsymbol{\varphi}(\mathbf{X}) = \mathbf{v}, \quad \delta p(\mathbf{X}) = 1, \quad \delta\Theta(\mathbf{X}) = 1 \tag{48}$$

which are admissible when $\Gamma_{\boldsymbol{\varphi}} = \emptyset$ (or when $\bar{\boldsymbol{\varphi}} = \mathbf{0}$). This choice shows that the time rate of change of the total energy is negative,

$$\begin{aligned}
\frac{\mathrm{d}}{\mathrm{d}t}\mathsf{H} &= \frac{\mathrm{d}}{\mathrm{d}t}\mathsf{T} + \frac{\mathrm{d}}{\mathrm{d}t}\mathsf{V} \\
&= \langle \mathbf{v}, \dot{\boldsymbol{\pi}} \rangle_{\Omega_0} + \int_{\Omega_0} [\dot{\tilde{W}}(\mathbf{b}^{\mathrm{e}}, \xi) + \dot{U}(\Theta)]\, \mathrm{d}\Omega_0 \\
&= \langle \mathbf{v}, \dot{\boldsymbol{\pi}} \rangle_{\Omega_0} + \int_{\Omega_0} [\mathrm{dev}\,\boldsymbol{\tau} : \mathbf{d} - \mathscr{D}^{\mathrm{int}} + U'(\Theta)\dot{\Theta}]\, \mathrm{d}\Omega_0 \quad \text{(by (24))} \\
&= \langle \mathbf{v}, \dot{\boldsymbol{\pi}} \rangle_{\Omega_0} + \int_{\Omega_0} [\mathrm{dev}\,\boldsymbol{\tau} : \mathbf{d} - \mathscr{D}^{\mathrm{int}} + p\dot{\Theta}]\, \mathrm{d}\Omega_0 \\
&= \langle \mathbf{v}, \dot{\boldsymbol{\pi}} \rangle_{\Omega_0} + \int_{\Omega_0} [\mathrm{dev}\,\boldsymbol{\tau} : \mathbf{d} + p\dot{J} - \mathscr{D}^{\mathrm{int}}]\, \mathrm{d}\Omega_0 \\
&= \langle \mathbf{v}, \dot{\boldsymbol{\pi}} \rangle_{\Omega_0} + \int_{\Omega_0} \left[\tfrac{1}{2}\boldsymbol{\varphi}^*(\mathrm{dev}\,\boldsymbol{\tau}) : \dot{\mathbf{C}} + p(\partial_{\mathbf{C}} J) : \dot{\mathbf{C}} - \mathscr{D}^{\mathrm{int}}\right] \mathrm{d}\Omega_0 \\
&= \langle \mathbf{v}, \dot{\boldsymbol{\pi}} \rangle_{\Omega_0} + \int_{\Omega_0} [[\boldsymbol{\varphi}^*(\mathrm{dev}\boldsymbol{\tau}) + 2p(\partial_{\mathbf{C}} J)] : \mathbf{F}^{\mathrm{T}}\dot{\mathbf{F}} - \mathscr{D}^{\mathrm{int}}]\, \mathrm{d}\Omega_0 \\
&= \langle \mathbf{v}, \dot{\boldsymbol{\pi}} \rangle_{\Omega_0} + \int_{\Omega_0} [\mathbf{FS} : \mathrm{GRAD}_{\mathbf{X}}[\mathbf{v}] - \mathscr{D}^{\mathrm{int}}]\, \mathrm{d}\Omega_0 \\
&= \langle \mathbf{v}, \dot{\boldsymbol{\pi}} \rangle_{\Omega_0} + \langle \mathrm{GRAD}_{\mathbf{X}}[\mathbf{v}], \mathbf{FS} \rangle_{\Omega_0} - \int_{\Omega_0} \mathscr{D}^{\mathrm{int}}\, \mathrm{d}\Omega_0 \\
&= -\int_{\Omega_0} \mathscr{D}^{\mathrm{int}}\, \mathrm{d}\Omega_0 \\
&\leqslant 0
\end{aligned} \tag{49}$$

□

The goal of this work is to construct a discrete MPM which also satisfies these conservation properties.

3. THE MATERIAL-POINT METHOD

Details about the MPM appear in References [1–3, 5]. The purpose of this section is to describe the MPM for the problem of Equation (13) with an emphasis on the changes required for the three-field, energy-consistent, hyperelastic-plastic formulation. First, the numerical integration of the plasticity equations is presented. Next, the concept of a discrete derivative is recalled, an essential part of the construction of an energy-consistent discretization. Then, the main steps in the MPM algorithm are summarized, indicating the time-stepping algorithm and mixed formulation. Finally, the conservation properties of the MPM algorithm are examined.

3.1. Numerical integration of plasticity equations

The material points act essentially as quadrature points for an MPM simulation, and as such the material stress response is computed using a strain-driven numerical algorithm at each of these points. In this regard MPM is virtually identical to the finite element method. Thus, at every material point of an MPM simulation, for every time step, the plasticity evolution equations must be integrated to yield updated material response information. The goal is to discretely integrate the plasticity evolution equations over a numerical time step $\Delta t > 0$, producing stresses and internal variables at time t_{n+1} from the initial conditions at time t_n, with $\Delta t := t_{n+1} - t_n$. The numerical algorithm for performing this update is discussed in this section and involves an operator splitting procedure.

3.1.1. Predictor–corrector algorithm. The constitutive model integration algorithm is designed to solve the plasticity evolution equations of Section 2.3.2. The first step in an operator split approach is the solution of the predictor phase. Assuming no plastic behaviour, the flow rules (28b) and (30) reduce to

$$\dot{\mathbf{G}}^{\mathrm{p}} = \mathbf{0} \quad \text{and} \quad \dot{\xi} = 0 \tag{50}$$

The solution to these equations is simply

$$\mathbf{G}^{\mathrm{p}^{\mathrm{tr}}}_{n+1} = \mathbf{G}^{\mathrm{p}}_{n} \quad \text{and} \quad \xi^{\mathrm{tr}}_{n+1} = \xi_n \tag{51}$$

where the superscript ‘tr’ indicates that these are the trial values of the plastic internal variables at time t_{n+1}. Define the trial stress as

$$\boldsymbol{\tau}^{\mathrm{tr}}_{n+1} := 2\mathbf{b}^{\mathrm{e}^{\mathrm{tr}}}_{n+1}\partial_{\mathbf{b}^{\mathrm{e}}} W(\mathbf{b}^{\mathrm{e}^{\mathrm{tr}}}_{n+1}, \xi^{\mathrm{tr}}_{n+1}) \tag{52}$$

the trial hardening variable as

$$q^{\mathrm{tr}}_{n+1} := -\partial_{\xi} W(\mathbf{b}^{\mathrm{e}^{\mathrm{tr}}}_{n+1}, \xi^{\mathrm{tr}}_{n+1}) \tag{53}$$

and the trial value of the yield function as $\Phi^{\mathrm{tr}}_{n+1} := \Phi(\boldsymbol{\tau}^{\mathrm{tr}}_{n+1}, q^{\mathrm{tr}}_{n+1})$. By checking the value of the yield function, the next step is determined:

$$\Phi^{\mathrm{tr}}_{n+1} < 0 \implies \text{elastic step}$$

$$\Phi^{\mathrm{tr}}_{n+1} > 0 \implies \text{plastic step}$$

If $\Phi^{\mathrm{tr}}_{n+1}<0$, simply set

$$\boldsymbol{\tau}_{n+1} = \boldsymbol{\tau}^{\mathrm{tr}}_{n+1}, \quad \mathbf{G}^{\mathrm{p}}_{n+1} = \mathbf{G}^{\mathrm{p}}_{n}, \quad \xi_{n+1} = \xi_n$$

If $\Phi^{\mathrm{tr}}_{n+1}>0$, the trial state is invalid and must be corrected.

The plastic corrector step is conducted by evaluating the flow rules (28b) and (30) assuming that $\dot{\gamma}>0$ so that

$$\dot{\mathbf{G}}^{\mathrm{p}} = -2\dot{\gamma}(\mathbf{F}^{-1}\mathbf{n}\mathbf{F})\mathbf{G}^{\mathrm{p}} \tag{54}$$

and

$$\dot{\xi} = \dot{\gamma}\partial_q \Phi \tag{55}$$

along with the yield condition

$$\dot{\gamma} = \frac{\Phi_{n+1}}{\eta} \tag{56}$$

Motivated by the developments in References [21, 22, 30, 31] a backward Euler exponential update in time produces the equation

$$\begin{aligned}\mathbf{G}^{\mathrm{p}}_{n+1} &= \exp(-2\dot{\gamma}_{n+1}\Delta t \mathbf{F}^{-1}_{n+1}\mathbf{n}_{n+1}\mathbf{F}_{n+1})\mathbf{G}^{\mathrm{p}^{\mathrm{tr}}}_{n+1} \\ &= \mathbf{F}^{-1}_{n+1}\exp(-2\Delta\gamma\mathbf{n}_{n+1})\mathbf{F}_{n+1}\mathbf{G}^{\mathrm{p}^{\mathrm{tr}}}_{n+1}\end{aligned} \tag{57}$$

where $\Delta\gamma := \dot{\gamma}_{n+1}\Delta t$. Given that $\mathbf{b}^{\mathrm{e}}_{n+1} = \mathbf{F}_{n+1}\mathbf{G}^{\mathrm{p}}_{n+1}\mathbf{F}^{\mathrm{T}}_{n+1}$, this may be written as

$$\mathbf{b}^{\mathrm{e}}_{n+1} = \exp(-2\Delta\gamma\mathbf{n}_{n+1})\mathbf{b}^{\mathrm{e}^{\mathrm{tr}}}_{n+1} \tag{58}$$

where $\mathbf{b}^{\mathrm{e}^{\mathrm{tr}}}_{n+1} = \mathbf{F}_{n+1}\mathbf{G}^{\mathrm{p}^{\mathrm{tr}}}_{n+1}\mathbf{F}^{\mathrm{T}}_{n+1}$. A backward Euler time discretization of the flow rule for ξ yields

$$\xi_{n+1} - \xi^{\mathrm{tr}}_{n+1} = \Delta\gamma \cdot \partial_q \Phi_{n+1} \tag{59}$$

and for the consistency condition is

$$\Delta\gamma = \Phi_{n+1}\frac{\Delta t}{\eta} \tag{60}$$

For isotropic models the implementation of the plasticity integrator may be done in terms of the principal Kirchhoff stresses β_A (the eigenvalues of $\boldsymbol{\tau}$) and the principal elastic logarithmic

stretches $\varepsilon_A^{\mathrm{e}}$ (the log of the eigenvalues of $\sqrt{\mathbf{b}^{\mathrm{e}}}$) [21, 22]. Thus, the plasticity update equations reduce to a (generally non-linear) set of algebraic equations in principal stress–strain space [27]:

$$\begin{aligned} \varepsilon_A^{\mathrm{e}} - \varepsilon_A^{\mathrm{e}^{\mathrm{tr}}} + \Delta\gamma \cdot (\partial_{\beta_A} \Phi_{n+1}) &= 0 \\ \beta_A - \partial_{\varepsilon_A^{\mathrm{e}}} W_{n+1} &= 0 \\ \xi_{n+1} - \xi_{n+1}^{\mathrm{tr}} - \Delta\gamma \cdot \partial_q \Phi_{n+1} &= 0 \\ \Phi_{n+1} - \frac{\eta}{\Delta t}\Delta\gamma &= 0 \end{aligned} \quad \text{for} \quad A = \{1, 2, 3\} \tag{61}$$

Note that these equations are well defined in the limit as $\eta \searrow 0$. For the J^2 plasticity model of Section 2.3.3, the set of equations is linear with a closed form solution

$$\Delta\gamma = \left[\frac{\eta}{\Delta t} + \frac{2}{3}H + 2G\right]^{-1} \Phi_{n+1}^{\mathrm{tr}} \tag{62}$$

3.1.2. Algorithmic dissipation. The construction of energy-consistent numerical methods for dissipative dynamical systems typically requires a consistent approximation for the energy dissipated during a time step. For the plasticity models under consideration this is not a difficult task. Assuming plastic flow and using Equation (39), a discrete backward Euler approximation to the internal dissipation is

$$\begin{aligned} \Delta\mathscr{D}^{\mathrm{int}} &:= \int_{t_n}^{t_{n+1}} \mathscr{D}^{\mathrm{int}} \, \mathrm{d}t \\ &= \int_{t_n}^{t_{n+1}} \dot{\gamma} \left[\Phi + \sqrt{\tfrac{2}{3}}\sigma_Y\right] \mathrm{d}t \\ &\approx \left[\Phi_{n+1} + \sqrt{\tfrac{2}{3}}\sigma_Y\right] \Delta\gamma \\ &= \left[\frac{\eta}{\Delta t}\Delta\gamma + \sqrt{\tfrac{2}{3}}\sigma_Y\right] \Delta\gamma \\ &\geqslant 0 \end{aligned} \tag{63}$$

Note that this approximation is defined as $\eta \searrow 0$. When there is no plastic flow $\Delta\mathscr{D}^{\mathrm{int}} = 0$. For more general plasticity models, Equation (29), for example, can be used to derive expressions for the algorithmic dissipation.

3.2. Discrete derivatives

A discrete derivative must approximate the analytical derivative and satisfy a directional derivative property, as specified in the following definition. The directional derivative property plays a key role in obtaining energy-consistent time discretizations.

Definition 3.1 (*(Discrete derivative) Gonzalez* [*32*])
Let $\mathbb{K} \subset \mathbb{R}^n$ be a convex set and assume there exists a smooth function $f : \mathbb{K} \to \mathbb{R}$. A *discrete derivative* $D_{\mathbf{z}} f : \mathbb{K} \times \mathbb{K} \to \mathbb{R}^n$ is a mapping such that

1. *Directionality*:

$$D_{\mathbf{z}} f(\mathbf{z}_1, \mathbf{z}_2) \cdot (\mathbf{z}_2 - \mathbf{z}_1) = f(\mathbf{z}_2) - f(\mathbf{z}_1) \quad \forall \mathbf{z}_1, \mathbf{z}_2 \in \mathbb{K}$$

2. *Consistency*:

$$D_{\mathbf{z}} f(\mathbf{z}_1, \mathbf{z}_2) = \partial_{\mathbf{z}} f(\bar{\mathbf{z}}) + \mathcal{O}(\|\mathbf{z}_2 - \mathbf{z}_1\|)$$

where $\bar{\mathbf{z}} := \frac{1}{2}(\mathbf{z}_1 + \mathbf{z}_2)$.

There is not a unique function which satisfies this definition. However, the construction adopted here is similar to that of References [8, 32]. The discrete derivative is evaluated as

$$D_{\mathbf{z}} f(\mathbf{z}_1, \mathbf{z}_2) := \overline{\partial_{\mathbf{z}} f} + \left[\frac{f(\mathbf{z}_2) - f(\mathbf{z}_1) - \overline{\partial_{\mathbf{z}} f}}{\|\mathbf{z}_2 - \mathbf{z}_1\|^2} \right] (\mathbf{z}_2 - \mathbf{z}_1) \tag{64}$$

where $\overline{\partial_{\mathbf{z}} f}$ satisfies

$$\overline{\partial_{\mathbf{z}} f} = \partial_{\mathbf{z}} f(\bar{\mathbf{z}}) + \mathcal{O}(\|\mathbf{z}_2 - \mathbf{z}_1\|) \tag{65}$$

Two possible options are

1. midpoint approximation:

$$\overline{\partial_{\mathbf{z}} f} := \partial_{\mathbf{z}} f(\bar{\mathbf{z}}) \tag{66}$$

   This is the form adopted in References [8, 32].
2. trapezoidal approximation:

$$\overline{\partial_{\mathbf{z}} f} := \tfrac{1}{2}[\partial_{\mathbf{z}} f(\mathbf{z}_1) + \partial_{\mathbf{z}} f(\mathbf{z}_2)] \tag{67}$$

Either option satisfies (65) and ensures that $D_{\mathbf{z}} f(\mathbf{z}_1, \mathbf{z}_2)$ has a well-defined limit as $\|\mathbf{z}_2 - \mathbf{z}_1\| \searrow 0$. If a positive term $\mathscr{D} > 0$ is added to (64) so that the discrete derivative has the modified form

$$D_{\mathbf{z}} f(\mathbf{z}_1, \mathbf{z}_2) := \overline{\partial_{\mathbf{z}} f} + \left[\frac{f(\mathbf{z}_2) - f(\mathbf{z}_1) + \mathscr{D} - \overline{\partial_{\mathbf{z}} f}}{\|\mathbf{z}_2 - \mathbf{z}_1\|^2} \right] (\mathbf{z}_2 - \mathbf{z}_1) \tag{68}$$

then

$$D_{\mathbf{z}} f(\mathbf{z}_1, \mathbf{z}_2) \cdot (\mathbf{z}_2 - \mathbf{z}_1) = f(\mathbf{z}_2) - f(\mathbf{z}_1) + \mathscr{D} \geqslant f(\mathbf{z}_2) - f(\mathbf{z}_1) \quad \forall \mathbf{z}_1, \mathbf{z}_2 \in \mathbb{K} \tag{69}$$

3.2.1. Algorithmic stress. The construction of energy-consistent numerical methods for plasticity typically requires the use of an appropriately defined stress tensor. Said tensor is generally

constructed so that the dissipation inequality is automatically satisfied in an algorithmically consistent manner. Towards that end, a symmetric *algorithmic stress* is defined as [9]

$$\mathbf{S}^{\text{dev}}_{\text{algo}} := \bar{\mathbf{S}} + \left[\frac{2(\tilde{W}(\mathbf{b}^{\text{e}}_{n+1}, \xi_{n+1}) - \tilde{W}(\mathbf{b}^{\text{e}}_{n}, \xi_{n}) + \Delta\mathscr{D}^{\text{int}}) - \bar{\mathbf{S}} : \Delta\mathbf{C}}{\|\Delta\mathbf{C}\|^2} \right] \Delta\mathbf{C} \tag{70}$$

where

$$\bar{\mathbf{S}} := \tfrac{1}{2}[\boldsymbol{\varphi}^{*}_{n}(\text{dev}\boldsymbol{\tau}_{n}) + \boldsymbol{\varphi}^{*}_{n+1}(\text{dev}\,\boldsymbol{\tau}_{n+1})] \tag{71}$$

This definition makes use of the notion of a discrete derivative of $\tilde{W}$ to define $\mathbf{S}^{\text{dev}}_{\text{algo}}$. Furthermore, the utility of the discrete derivative is seen in the following easily verified inequality

$$\tfrac{1}{2}\mathbf{S}^{\text{dev}}_{\text{algo}} : \Delta\mathbf{C} = \Delta\tilde{W} + \Delta\mathscr{D}^{\text{int}} \geqslant \Delta\tilde{W} \tag{72}$$

Thus, $\mathbf{S}^{\text{dev}}_{\text{algo}}$ satisfies by construction a time-discrete form of the dissipation inequality (24) and shall be used, along with discrete derivatives of $J(\mathbf{C})$ and $U(\Theta)$, to ensure energy consistency of the dynamic MPM time-stepping algorithm for (13).

Remark 3.1

1. The addition of a dissipation term $\mathscr{D}>0$ to the discrete derivative has been used previously in References [33, 34] to add controllable high-frequency dissipation to dynamic hyperelastic simulations.
2. In a seminal work, Meng and Laursen [9] consider a very similar formulation for dynamic finite deformation plasticity in a Lagrangian finite element setting. However, in that paper the authors make use of a midpoint integrator [21] for the plastic evolution equations. Consequently, the definition of $\bar{\mathbf{S}}$ takes the form

   $$\bar{\mathbf{S}} := \boldsymbol{\varphi}^{*}_{n+1/2}(\text{dev}\,\boldsymbol{\tau}_{n+1/2})$$

   which in the purely elastic case collapses to

   $$\bar{\mathbf{S}} = 2\partial_{\mathbf{C}}\hat{W}(\mathbf{F}^{\text{T}}_{n+1/2}\mathbf{F}_{n+1/2})$$

   Unfortunately, this form for $\bar{\mathbf{S}}$ may not have a well-defined limit as $\|\Delta\mathbf{C}\| \searrow 0$ (see Reference [5]). To avoid this possible problem, and for ease of implementation, a backward Euler integrator along with Equation (71) is chosen for this work.
3. The general developments presented here are not restricted to isotropic multiplicative plasticity. The same algorithmic constructions can be applied to any hyperelastic-based, thermodynamically consistent material model. This includes, but is not limited to, additive Green–Naghdi plasticity References [9, 35], finite strain viscoelasticity [36], anisotropic single crystal plasticity [37, 38] and continuum damage modelling [39, 40].

3.3. Discrete equations of motion

The purpose of this section is to present the time and space discrete MPM equations of motion. The method is very similar to a standard finite element approximation of the weak form (13). However, for an MPM simulation an additional projection step is required and an

additional regrid step is optional. The notation used in this section is generally consistent with the notation typically seen in books and papers on the finite element method. The numerical implementation of the plasticity model has already been presented, and is exactly the same strain-driven algorithm used in Lagrangian finite element simulations.

MPM consists of a set of material points and a background grid or mesh. Let $N_{\text{pt}}>0$ denote the number of material points of the discrete simulation, and let $N_{\text{nodes}}>0$ denote the number of nodes of the background mesh. Any quantity associated with a material point is identified by a superscript $(\cdot)^{\text{pt}}$. For example, the velocity of a material point is notated as $\mathbf{v}^{\text{pt}}$. Any quantity associated with the background mesh is identified by a superscript $(\cdot)^h$, with $h>0$ denoting the mesh size, or by indexes $\{A, B, C \ldots\}$ indicating nodal values. For example, $\mathbf{v}^h(\mathbf{x})$ is the velocity field of the mesh with nodal values $\mathbf{v}_A$ for $A \in \{1, 2, \ldots, N_{\text{nodes}}\}$. (In a slight abuse of notation, $(\cdot)^h$ is also used to notate the vector of nodal values of $(\cdot)$. This should not cause the reader any confusion in the context where it is used.) A subscript $(\cdot)_{n+1}$ indicates the time-step index, corresponding to a solution at time t_{n+1}. A capital Δ is used to indicate a time-step increment in a quantity, $\Delta(\cdot) = (\cdot)_{n+1} - (\cdot)_n$, and in standard fashion, $(\cdot)_{n+\alpha} := (1-\alpha)(\cdot)_n + \alpha(\cdot)_{n+1} \forall \alpha \in [0, 1]$.

Denote by N^A the shape function of node A of the mesh. Let $\mathscr{W}^h \subset \mathscr{W}$ denote a typical finite-dimensional finite element subspace of $\mathscr{W}$, with corresponding solution space $\mathscr{S}^h \subset \mathscr{S}$. Then, for example, any $\delta\boldsymbol{\varphi}^h \in \mathscr{W}^h$ takes the form

$$\delta\boldsymbol{\varphi}^h(\mathbf{x}) = \sum_{A=1}^{N_{\text{nodes}}} N^A(\mathbf{x}) \delta\boldsymbol{\varphi}_A \tag{73}$$

All integrals are evaluated by treating the material points as quadrature points. For example, the second term in (13a) can be approximated as

$$\begin{gathered} \mathbf{B}^h(\mathbf{x}) := \text{GRAD}_{\mathbf{X}}[\delta\boldsymbol{\varphi}^h(\mathbf{x})] = \sum_{A=1}^{N_{\text{nodes}}} \delta\boldsymbol{\varphi}_A \otimes (\mathbf{F}_n^{\text{T}}(\mathbf{x}) \, \text{grad}_n[N^A(\mathbf{x})]) \\ \langle \text{GRAD}_{\mathbf{X}}[\delta\boldsymbol{\varphi}], \mathbf{F}_{n+\alpha}\mathbf{S} \rangle_{\Omega_0} \approx \sum_{\text{pt}=1}^{N_{\text{pt}}} (\mathbf{B}^h(\mathbf{x}_n^{\text{pt}}) : \mathbf{F}_{n+\alpha}^{\text{pt}} \mathbf{S}^{\text{pt}}) \Omega_0^{\text{pt}} \end{gathered} \tag{74}$$

where $\mathbf{x}_n^{\text{pt}} = \boldsymbol{\varphi}_n^{\text{pt}}$ is the material-point position at time step n and $\Omega_0^{\text{pt}}>0$ is the material volume associated with the material point pt. The transformation $\text{GRAD}_{\mathbf{X}}[\cdot] = \mathbf{F}_n^{\text{T}} \text{grad}_n[\cdot]$ is also used, where grad_n indicates the gradient with respect to the configuration at time t_n. Figure 1 schematically shows the notation used to relate the reference configuration of the deforming body with its configuration at times t_n and t_{n+1}.

The mass $m^{\text{pt}} = \rho_0(\mathbf{x}^{\text{pt}})\Omega_0^{\text{pt}} > 0$ is constant for each material point. The material-point momentum is then $\boldsymbol{\pi}^{\text{pt}} := m^{\text{pt}} \mathbf{v}^{\text{pt}}$. Using the material-point masses, the *consistent* mass matrix $\mathbf{M}$ is defined with nodal components

$$M^{AB} := \sum_{\text{pt}=1}^{N_{\text{pt}}} m^{\text{pt}} N^A(\mathbf{x}^{\text{pt}}) N^B(\mathbf{x}^{\text{pt}}) \approx \int_{\Omega_0} \rho_0 N^A N^B \, \text{d}\Omega_0 \tag{75}$$

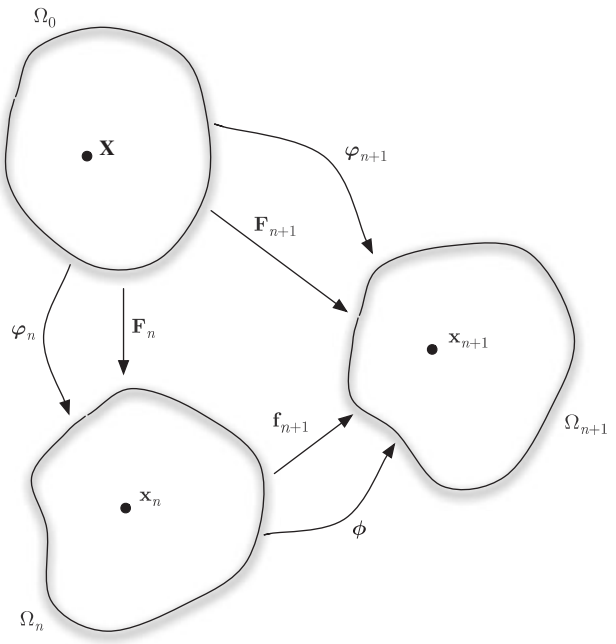

Figure 1. Diagram indicating the notation used to relate the reference configuration of the body with its configuration at times t_n and t_{n+1}. By this construction, $\boldsymbol{\varphi}_{n+1} = \boldsymbol{\phi} \circ \boldsymbol{\varphi}_n$ and $\mathbf{F}_{n+1} = \mathbf{f}_{n+1}\mathbf{F}_n$. Assuming the same fixed Cartesian co-ordinate system for all three configurations, $\boldsymbol{\phi} = \mathbf{id} + \Delta\boldsymbol{\varphi}$, where $\Delta\boldsymbol{\varphi} = (\boldsymbol{\varphi}_{n+1} - \boldsymbol{\varphi}_n) \circ \boldsymbol{\varphi}_n^{-1}$.

Remark 3.2
Many MPM implementations use a lumped mass matrix [1–4, 6, 41]. However, in an effort to ensure that global conservation properties are satisfied [5, 10], only the consistent mass matrix is considered in this work.

Given the material-point data $\{\boldsymbol{\varphi}_n^{\mathrm{pt}}, \mathbf{v}_n^{\mathrm{pt}}, \mathbf{F}_n^{\mathrm{pt}}, \Theta_n^{\mathrm{pt}}, \mathbf{G}_n^{\mathrm{p}}, \xi_n\}$ at time t_n, the goal is to determine the material-point data $\{\boldsymbol{\varphi}_{n+1}^{\mathrm{pt}}, \mathbf{v}_{n+1}^{\mathrm{pt}}, \mathbf{F}_{n+1}^{\mathrm{pt}}, \Theta_{n+1}^{\mathrm{pt}}, \mathbf{G}_{n+1}^{\mathrm{p}}, \xi_{n+1}\}$ at time $t_{n+1} := t_n + \Delta t$. Assuming a background finite element mesh exists, the MPM algorithm is as follows:

Algorithm MPM

The algorithm consists of four primary steps:

1. *Material-point-to-grid projection*. Compute the consistent mass matrix $\mathbf{M}_n$ using (75). Compute the grid velocities $\mathbf{v}_n^h$ such that

$$\sum_{B=1}^{N_{\mathrm{nodes}}} M_n^{AB}\mathbf{v}_{B,n} = \sum_{\mathrm{pt}=1}^{N_{\mathrm{pt}}} N^A(\mathbf{x}_n^{\mathrm{pt}})\boldsymbol{\pi}_n^{\mathrm{pt}} \quad \forall A \in \{1, 2, \ldots, N_{\mathrm{nodes}}\} \tag{76}$$

2. *Lagrangian mesh dynamics*. Solve the non-linear algebraic equations

$$\frac{1}{\Delta t}\sum_{B=1}^{N_{\text{nodes}}} M_n^{AB}(\mathbf{v}_{B,n+1}-\mathbf{v}_{B,n}) + (\mathbf{F}^{\text{int}})^A_{n+1/2} - (\mathbf{F}^{\text{ext}})^A_{n+1/2} = \mathbf{0} \tag{77a}$$

$$\frac{1}{\Delta t}\Delta\boldsymbol{\varphi}_A = \mathbf{v}_{A,n+1/2} \tag{77b}$$

$$\sum_{\text{pt}=1}^{N_{\text{pt}}} \delta\theta^h(\boldsymbol{\varphi}_n^{\text{pt}})\cdot[p^h(\boldsymbol{\varphi}_n^{\text{pt}}) - D_\Theta U(\Theta_n^{\text{pt}},\Theta_{n+1}^{\text{pt}})]\Omega_0^{\text{pt}} = 0 \tag{77c}$$

$$\sum_{\text{pt}=1}^{N_{\text{pt}}} \delta p^h(\boldsymbol{\varphi}_n^{\text{pt}})\cdot[\theta^h(\boldsymbol{\varphi}_n^{\text{pt}}) - \Delta J^{\text{pt}}]\Omega_0^{\text{pt}} = 0 \tag{77d}$$

$$\Theta_{n+1}^{\text{pt}} = \Theta_n^{\text{pt}} + \theta^h(\boldsymbol{\varphi}_n^{\text{pt}}) \tag{77e}$$

for $A\in\{1,2,\ldots,N_{\text{nodes}}\}$, where $(\mathbf{F}^{\text{int}})^A_{n+1/2}$ and $(\mathbf{F}^{\text{ext}})^A_{n+1/2}$ are the internal and external forces, respectively, associated with node A at time $t_{n+1/2}$. These forces are defined as

$$\begin{aligned}(\mathbf{F}^{\text{int}})^A_{n+1/2} &:= \sum_{\text{pt}=1}^{N_{\text{pt}}} (\mathbf{F}^{\text{pt}}_{n+1/2}\mathbf{S}^h)(\mathbf{F}^{\text{pt}}_n)^{\text{T}}\text{grad}_n[N^A(\mathbf{x}_n^{\text{pt}})]\Omega_0^{\text{pt}}\\ &\approx \int_{\Omega_0}(\mathbf{F}_{n+1/2}\mathbf{S}^h)\text{GRAD}_{\mathbf{X}}[N^A]\,\text{d}\Omega_0\end{aligned} \tag{78a}$$

$$\begin{aligned}(\mathbf{F}^{\text{ext}})^A_{n+1/2} &:= \sum_{\text{pt}=1}^{N_{\text{pt}}} m^{\text{pt}}\mathbf{b}_{n+1/2}N^A(\mathbf{x}_n^{\text{pt}}) + \bar{\mathbf{T}}^A_{n+1/2}\\ &\approx \int_{\Omega_0} N^A\rho_0\mathbf{b}_{n+1/2}\,\text{d}\Omega_0 + \int_{\Gamma_{\boldsymbol{\sigma}}} N^A\bar{\mathbf{T}}_{n+1/2}\,\text{d}\Gamma_0\end{aligned} \tag{78b}$$

where

$$\mathbf{S}^h := \mathbf{S}^{\text{dev}}_{\text{algo}} + 2p^h(\boldsymbol{\varphi}_n^{\text{pt}})\cdot D_{\mathbf{C}}J(\mathbf{C}_n^{\text{pt}},\mathbf{C}_{n+1}^{\text{pt}}) \tag{79}$$

and $\bar{\mathbf{T}}^A_{n+1/2}$ is an approximation to the nodal value of the surface traction, $\bar{\mathbf{T}}^A_{n+1/2}\approx\int_{\Gamma_{\boldsymbol{\sigma}}}N^A\bar{\mathbf{T}}_{n+1/2}\,\text{d}\Gamma_0$. The mixed variational fields $\{p^h,\theta^h\}$ are *not material-point based*. In an effort to avoid an overconstrained pressure field, which can lead to locking of a finite element approximation, $\{p^h,\theta^h\}$ and their corresponding variations are chosen to be *piecewise constant* on each background finite element [17]. Note that

$$\sum_{\text{pt}=1}^{N_{\text{pt}}} \delta\theta^h(\boldsymbol{\varphi}_n^{\text{pt}})\cdot[p^h(\boldsymbol{\varphi}_n^{\text{pt}}) - D_\Theta U(\Theta_n^{\text{pt}},\Theta_{n+1}^{\text{pt}})]\Omega_0^{\text{pt}} \approx \langle\delta\theta,\, p - D_\Theta U(\Theta_n,\Theta_{n+1})\rangle_{\Omega_0}$$

and

$$\sum_{\mathrm{pt}=1}^{N_{\mathrm{pt}}} \delta p^h(\boldsymbol{\varphi}_n^{\mathrm{pt}}) \cdot [\theta^h(\boldsymbol{\varphi}_n^{\mathrm{pt}}) - \Delta J^{\mathrm{pt}}]\Omega_0^{\mathrm{pt}} \approx \langle \delta p, \theta - \Delta J \rangle_{\Omega_0}$$

Note also the use of the discrete derivatives $D_\Theta U$, $D_{\mathbf{C}} J$ and $\mathbf{S}^{\mathrm{dev}}_{\mathrm{algo}}$. During this step, the deformation gradient for each material point is multiplicatively updated via

$$\begin{aligned} \mathbf{f}^h_{n+1}(\mathbf{x}_n) &:= \mathbf{I} + \mathrm{grad}_n[\Delta\boldsymbol{\varphi}^h(\mathbf{x}_n)] \\ \mathbf{F}^{\mathrm{pt}}_{n+1} &:= \mathbf{f}^h_{n+1}(\mathbf{x}^{\mathrm{pt}}_n)\mathbf{F}^{\mathrm{pt}}_n \end{aligned} \tag{80}$$

and the plasticity integration is performed at each material point (Section 3.1). The above equations of this step, all together, are the Galerkin spatial projection of the weak form (13) onto the finite element subspace, coupled with an incremental midpoint-based time-stepping scheme.

3. *Material-point update*. Update the material-point positions and velocities via

$$\begin{aligned} \boldsymbol{\varphi}^{\mathrm{pt}}_{n+1} &= \boldsymbol{\varphi}^{\mathrm{pt}}_n + \Delta\boldsymbol{\varphi}^h(\mathbf{x}^{\mathrm{pt}}_n) \\ \mathbf{v}^{\mathrm{pt}}_{n+1} &= \mathbf{v}^{\mathrm{pt}}_n + \Delta\mathbf{v}^h(\mathbf{x}^{\mathrm{pt}}_n) \end{aligned} \tag{81}$$

4. *Regrid*. During step 2, the finite element mesh deforms. During step 4, the mesh may be moved, if desired. In particular, the mesh may be returned to the position it occupied at the beginning of step 2. This choice is typical of many MPM implementations. Alternatively, the mesh may be redefined to suit any requirements the user may have, including the enforcement of Dirichlet boundary conditions, or adaption to features of the solution.

Remark 3.3

1. Equations (77a) and (77b) are typical of many finite element and MPM simulations. Equations (77c)–(77e) for the mixed variational fields are not typically seen in MPM formulations. Additionally, the use of discrete derivatives is also not commonly observed within the MPM and particle method community. These two modifications represent important changes relative to standard MPM approaches.
2. Equations (77c)–(77e) are solved at the element level and do not explicitly enter the global system of Equations (77a) [17].
3. Equations (77d)–(77e) are not necessarily the only method for updating the element level mixed volume. Alternative formulations are discussed in Appendix A. Unfortunately, the energy conservation properties of the alternatives are unclear.
4. The four-node constant pressure/volume quadrilateral (Q1/P0) finite element *does not satisfy the inf–sup*(*LBB*) *condition* [42]. The existence of well-known pressure *checkerboard modes* [43, 44] precludes satisfaction of the LBB stability criterion. However, this ill-conditioning appears to be restricted to the pressure field and the velocity field is

very often still convergent (Theorem 10.3.7 of Reference [45] and Reference [46]). A convergent pressure field can often be recovered by filtering or smoothing the oscillatory pressures [46–50]. Despite this shortcoming, the Q1/P0 quadrilateral remains popular in computational solid mechanics and is a relatively simple element formulation which avoids volumetric locking.

3.4. Conservation properties

The goal of the MPM time-stepping scheme is to mimic the conservation properties of the continuum. The total particle linear momentum and the total particle angular momentum should be exactly conserved. The total particle internal energy should be consistently dissipated. After defining these discrete integrals of the motion, it is shown that Algorithm MPM does in fact possess the desired conservation properties.

Definition 3.2
The *total grid (mesh) linear momentum* $\mathbf{L}^h$ is defined as

$$\mathbf{L}^h := \sum_{A=1}^{N_{\text{nodes}}} \left(\sum_{B=1}^{N_{\text{nodes}}} M^{AB} \mathbf{v}_B \right) \tag{82}$$

Definition 3.3
The *total material-point linear momentum* $\mathbf{L}^{\text{pt}}$ is defined as

$$\mathbf{L}^{\text{pt}} := \sum_{\text{pt}=1}^{N_{\text{pt}}} \boldsymbol{\pi}^{\text{pt}} \tag{83}$$

Definition 3.4
The *total grid (mesh) angular momentum* $\mathbf{J}^h$ is defined as

$$\mathbf{J}^h := \sum_{A=1}^{N_{\text{nodes}}} \left(\boldsymbol{\varphi}_A \times \sum_{B=1}^{N_{\text{nodes}}} M^{AB} \mathbf{v}_B \right) \tag{84}$$

Definition 3.5
The *total material-point angular momentum* $\mathbf{J}^{\text{pt}}$ is defined as

$$\mathbf{J}^{\text{pt}} := \sum_{\text{pt}=1}^{N_{\text{pt}}} (\boldsymbol{\varphi}^{\text{pt}} \times \boldsymbol{\pi}^{\text{pt}}) = \sum_{\text{pt}=1}^{N_{\text{pt}}} (\mathbf{x}^{\text{pt}} \times \boldsymbol{\pi}^{\text{pt}}) \tag{85}$$

Definition 3.6
The *total grid (mesh) kinetic energy* T^h is defined as

$$2\mathsf{T}^h := \sum_{A=1}^{N_{\text{nodes}}} \left(\mathbf{v}_A \cdot \sum_{B=1}^{N_{\text{nodes}}} M^{AB} \mathbf{v}_B \right) \tag{86}$$

Definition 3.7
The *total material-point kinetic energy* T^{pt} is defined as

$$2\mathsf{T}^{\mathrm{pt}} := \sum_{\mathrm{pt}=1}^{N_{\mathrm{pt}}} \left(\boldsymbol{\pi}^{\mathrm{pt}} \cdot \tfrac{1}{m^{\mathrm{pt}}}\boldsymbol{\pi}^{\mathrm{pt}}\right) = \sum_{\mathrm{pt}=1}^{N_{\mathrm{pt}}} (\boldsymbol{\pi}^{\mathrm{pt}} \cdot \mathbf{v}^{\mathrm{pt}}) = \sum_{\mathrm{pt}=1}^{N_{\mathrm{pt}}} m^{\mathrm{pt}} \|\mathbf{v}^{\mathrm{pt}}\|^2 \tag{87}$$

Definition 3.8
The *total material-point potential energy* V^{pt} is defined as

$$\mathsf{V}^{\mathrm{pt}} := \sum_{\mathrm{pt}=1}^{N_{\mathrm{pt}}} [\tilde{W}(\mathbf{b}^{\mathrm{e}}, \xi) + U(\Theta^{\mathrm{pt}})]\, \Omega_0^{\mathrm{pt}} \tag{88}$$

Definition 3.9
The *total grid (mesh) energy* H^h is defined as

$$\mathsf{H}^h := \mathsf{T}^h + \mathsf{V}^{\mathrm{pt}} \tag{89}$$

Definition 3.10
The *total material-point energy* H^{pt} is defined as

$$\mathsf{H}^{\mathrm{pt}} := \mathsf{T}^{\mathrm{pt}} + \mathsf{V}^{\mathrm{pt}} \tag{90}$$

Remark 3.4
There is no need to draw a distinction between total potential energy defined on the grid and total potential energy defined on the material points. They are in fact the same quantity. To compute the total grid potential energy one would use the material points as quadrature points for the integral, and the result would be exactly V^{pt}.

Linear and angular momentum conservation are fairly straightforward and the fact that these quantities are conserved has been shown previously in References [5, 8, 29].

Proposition 3.1
Assume $(\mathbf{F}^{\mathrm{ext}})^A_{n+1/2} = \mathbf{0}$. Then the mesh dynamics conserve exactly the total mesh linear momentum and total mesh angular momentum. Additionally, assume that the algorithmic stress satisfies the discrete dissipation inequality (72). Then the mesh dynamics dissipate the total mesh energy,

$$\mathsf{H}^h_{n+1} = \mathsf{H}^h_n - \sum_{\mathrm{pt}=1}^{N_{\mathrm{pt}}} \Delta\mathscr{D}^{\mathrm{int}} \cdot \Omega_0^{\mathrm{pt}} \leqslant \mathsf{H}^h_n \tag{91}$$

so that $\Delta\mathsf{H}^h = \Delta\mathsf{T}^h + \Delta\mathsf{V}^h \leqslant 0$.

Proof

1. *Linear momentum is conserved*. See References [5, 8].
2. *Angular momentum is conserved*. This is a direct consequence of the symmetry of $\mathbf{S}^h$ [5, 8].

3. *Energy is dissipated*. The presentation follows closely that of Proposition 5 in Reference [8]. First, since $\mathbf{M}$ is symmetric, note that the change in kinetic energy can be written as

$$\begin{aligned}\Delta \mathsf{T}^h &= \mathsf{T}^h_{n+1} - \mathsf{T}^h_n \\ &= \tfrac{1}{2}\sum_{A,B=1}^{N_{\text{nodes}}} (\mathbf{v}_{A,n} + \mathbf{v}_{A,n+1}) \cdot M_n^{AB}(\mathbf{v}_{B,n+1} - \mathbf{v}_{B,n}) \\ &= \sum_{A,B=1}^{N_{\text{nodes}}} \mathbf{v}_{A,n+1/2} \cdot M_n^{AB}(\mathbf{v}_{B,n+1} - \mathbf{v}_{B,n}) \end{aligned} \tag{92}$$

Use Equations (77c)–(77e) (72) (79):

$$\begin{aligned}\Delta \mathsf{V}^{\text{pt}} &= \mathsf{V}^{\text{pt}}_{n+1} - \mathsf{V}^{\text{pt}}_n \\ &= \sum_{\text{pt}=1}^{N_{\text{pt}}} [\tilde{W}(\mathbf{b}^{\text{e}}_{n+1}, \xi_{n+1}) + U(\Theta^{\text{pt}}_{n+1}) - \tilde{W}(\mathbf{b}^{\text{e}}_n, \xi_n) - U(\Theta^{\text{pt}}_n)]\Omega^{\text{pt}}_0 \\ &= \sum_{\text{pt}=1}^{N_{\text{pt}}} \left[\tfrac{1}{2}(\mathbf{C}^{\text{pt}}_{n+1} - \mathbf{C}^{\text{pt}}_n) : \mathbf{S}^{\text{dev}}_{\text{algo}} + D_\Theta U(\Theta^{\text{pt}}_n, \Theta^{\text{pt}}_n) \cdot \Delta\Theta^{\text{pt}} - \Delta\mathscr{D}^{\text{int}}\right]\Omega^{\text{pt}}_0 \\ &= \sum_{\text{pt}=1}^{N_{\text{pt}}} \left[\tfrac{1}{2}(\mathbf{C}^{\text{pt}}_{n+1} - \mathbf{C}^{\text{pt}}_n) : \mathbf{S}^{\text{dev}}_{\text{algo}} + p^h(\boldsymbol{\varphi}^{\text{pt}}_n) \cdot \theta^h(\boldsymbol{\varphi}^{\text{pt}}_n) - \Delta\mathscr{D}^{\text{int}}\right]\Omega^{\text{pt}}_0 \\ &= \sum_{\text{pt}=1}^{N_{\text{pt}}} \left[\tfrac{1}{2}(\mathbf{C}^{\text{pt}}_{n+1} - \mathbf{C}^{\text{pt}}_n) : \mathbf{S}^{\text{dev}}_{\text{algo}} + p^h(\boldsymbol{\varphi}^{\text{pt}}_n) \cdot \Delta J^{\text{pt}} - \Delta\mathscr{D}^{\text{int}}\right]\Omega^{\text{pt}}_0 \\ &= \sum_{\text{pt}=1}^{N_{\text{pt}}} \left[\tfrac{1}{2}(\mathbf{C}^{\text{pt}}_{n+1} - \mathbf{C}^{\text{pt}}_n) : \mathbf{S}^{\text{dev}}_{\text{algo}}\right]\Omega^{\text{pt}}_0 \\ &\quad + \sum_{\text{pt}=1}^{N_{\text{pt}}} \left[\tfrac{1}{2}(\mathbf{C}^{\text{pt}}_{n+1} - \mathbf{C}^{\text{pt}}_n) : 2p^h(\boldsymbol{\varphi}^{\text{pt}}_n) \cdot D_{\mathbf{C}} J(\mathbf{C}^{\text{pt}}_n, \mathbf{C}^{\text{pt}}_{n+1}) - \Delta\mathscr{D}^{\text{int}}\right]\Omega^{\text{pt}}_0 \\ &= \sum_{\text{pt}=1}^{N_{\text{pt}}} \left[\tfrac{1}{2}(\mathbf{C}^{\text{pt}}_{n+1} - \mathbf{C}^{\text{pt}}_n) : \mathbf{S}^h - \Delta\mathscr{D}^{\text{int}}\right]\Omega^{\text{pt}}_0 \end{aligned} \tag{93}$$

Note that several steps above make use of the directional property of the discrete derivative

$$\begin{aligned}\tilde{W}(\mathbf{b}^{\text{e}}_{n+1}, \xi_{n+1}) - \tilde{W}(\mathbf{b}^{\text{e}}_n, \xi_n) &= \tfrac{1}{2}\mathbf{S}^{\text{dev}}_{\text{algo}} : (\mathbf{C}_{n+1} - \mathbf{C}_n) \\ U(\Theta_{n+1}) - U(\Theta_n) &= D_\Theta U(\Theta_n, \Theta_n) \cdot (\Theta_{n+1} - \Theta_n) \\ J_{n+1} - J_n &= D_{\mathbf{C}} J(\mathbf{C}_n, \mathbf{C}_{n+1}) : (\mathbf{C}_{n+1} - \mathbf{C}_n) \end{aligned} \tag{94}$$

Continuing,

$$\Delta \mathsf{V}^{\mathrm{pt}} = \sum_{\mathrm{pt}=1}^{N_{\mathrm{pt}}} \left[\frac{1}{2} \left(\mathbf{C}_{n+1}^{\mathrm{pt}} - \mathbf{C}_{n}^{\mathrm{pt}} + \underbrace{(\mathbf{F}_{n}^{\mathrm{pt}})^{\mathrm{T}} \mathbf{F}_{n+1}^{\mathrm{pt}} - (\mathbf{F}_{n+1}^{\mathrm{pt}})^{\mathrm{T}} \mathbf{F}_{n}^{\mathrm{pt}}}_{\text{skew}} \right) : \mathbf{S}^{h} - \Delta \mathscr{D}^{\mathrm{int}} \right] \Omega_{0}^{\mathrm{pt}}$$

$$= \sum_{\mathrm{pt}=1}^{N_{\mathrm{pt}}} \left[\tfrac{1}{2} (\mathbf{F}_{n}^{\mathrm{pt}} + \mathbf{F}_{n+1}^{\mathrm{pt}})^{\mathrm{T}} (\mathbf{F}_{n+1}^{\mathrm{pt}} - \mathbf{F}_{n}^{\mathrm{pt}}) : \mathbf{S}^{h} - \Delta \mathscr{D}^{\mathrm{int}} \right] \Omega_{0}^{\mathrm{pt}}$$

$$= \sum_{\mathrm{pt}=1}^{N_{\mathrm{pt}}} [(\mathbf{F}_{n+1}^{\mathrm{pt}} - \mathbf{F}_{n}^{\mathrm{pt}}) : \mathbf{F}_{n+1/2}^{\mathrm{pt}} \mathbf{S}^{h} - \Delta \mathscr{D}^{\mathrm{int}}] \Omega_{0}^{\mathrm{pt}}$$

$$= \sum_{\mathrm{pt}=1}^{N_{\mathrm{pt}}} [\mathrm{grad}_{n}[\Delta \boldsymbol{\varphi}^{h}(\mathbf{x}_{n}^{\mathrm{pt}})] \mathbf{F}_{n}^{\mathrm{pt}} : \mathbf{F}_{n+1/2}^{\mathrm{pt}} \mathbf{S}^{h} - \Delta \mathscr{D}^{\mathrm{int}}] \Omega_{0}^{\mathrm{pt}}$$

$$= \sum_{\mathrm{pt}=1}^{N_{\mathrm{pt}}} \sum_{A=1}^{N_{\mathrm{nodes}}} ([\Delta \boldsymbol{\varphi}_{A} \otimes \mathrm{grad}_{n}[N^{A}(\mathbf{x}_{n}^{\mathrm{pt}})]] \mathbf{F}_{n}^{\mathrm{pt}}) : (\mathbf{F}_{n+1/2}^{\mathrm{pt}} \mathbf{S}^{h}) \Omega_{0}^{\mathrm{pt}} - \sum_{\mathrm{pt}=1}^{N_{\mathrm{pt}}} \Delta \mathscr{D}^{\mathrm{int}} \Omega_{0}^{\mathrm{pt}}$$

$$= \sum_{A=1}^{N_{\mathrm{nodes}}} \sum_{\mathrm{pt}=1}^{N_{\mathrm{pt}}} \Delta \boldsymbol{\varphi}_{A} \cdot (\mathbf{F}_{n+1/2}^{\mathrm{pt}} \mathbf{S}^{h}) \underbrace{(\mathbf{F}_{n}^{\mathrm{pt}})^{\mathrm{T}} \mathrm{grad}_{n}[N^{A}(\mathbf{x}_{n}^{\mathrm{pt}})]}_{\mathrm{GRAD}_{\mathbf{X}}[N^{A}(\mathbf{x}_{n}^{\mathrm{pt}})]} \Omega_{0}^{\mathrm{pt}} - \sum_{\mathrm{pt}=1}^{N_{\mathrm{pt}}} \Delta \mathscr{D}^{\mathrm{int}} \Omega_{0}^{\mathrm{pt}}$$

$$= \sum_{A=1}^{N_{\mathrm{nodes}}} \mathbf{v}_{A,n+1/2} \Delta t \cdot \sum_{\mathrm{pt}=1}^{N_{\mathrm{pt}}} (\mathbf{F}_{n+1/2}^{\mathrm{pt}} \mathbf{S}^{h}) (\mathbf{F}_{n}^{\mathrm{pt}})^{\mathrm{T}} \mathrm{grad}_{n}[N^{A}(\mathbf{x}_{n}^{\mathrm{pt}})] \Omega_{0}^{\mathrm{pt}} - \sum_{\mathrm{pt}=1}^{N_{\mathrm{pt}}} \Delta \mathscr{D}^{\mathrm{int}} \Omega_{0}^{\mathrm{pt}}$$

$$= \Delta t \sum_{A=1}^{N_{\mathrm{nodes}}} \mathbf{v}_{A,n+1/2} \cdot (\mathbf{F}^{\mathrm{int}})_{n+1/2}^{A} - \sum_{\mathrm{pt}=1}^{N_{\mathrm{pt}}} \Delta \mathscr{D}^{\mathrm{int}} \Omega_{0}^{\mathrm{pt}} \tag{95}$$

Finally, consideration of Equation (77a) yields

$$0 = \sum_{A=1}^{N_{\mathrm{Nodes}}} \mathbf{v}_{A,n+1/2} \cdot \left[\frac{1}{\Delta t} \sum_{B=1}^{N_{\mathrm{Nodes}}} M_{n}^{AB} (\mathbf{v}_{B,n+1} - \mathbf{v}_{B,n}) + (\mathbf{F}^{\mathrm{int}})_{n+1/2}^{A} \right]$$

$$= \frac{1}{\Delta t} (\mathsf{T}_{n+1}^{h} - \mathsf{T}_{n}^{h}) + \frac{1}{\Delta t} (\mathsf{V}_{n+1}^{\mathrm{pt}} - \mathsf{V}_{n}^{\mathrm{pt}}) + \frac{1}{\Delta t} \sum_{\mathrm{pt}=1}^{N_{\mathrm{pt}}} \Delta \mathscr{D}^{\mathrm{int}} \Omega_{0}^{\mathrm{pt}}$$

$$= \frac{1}{\Delta t} (\mathsf{H}_{n+1}^{h} - \mathsf{H}_{n}^{h}) + \frac{1}{\Delta t} \sum_{\mathrm{pt}=1}^{N_{\mathrm{pt}}} \Delta \mathscr{D}^{\mathrm{int}} \Omega_{0}^{\mathrm{pt}} \tag{96}$$

Since $\Delta t > 0$, $\mathsf{H}_{n+1}^{h} \leqslant \mathsf{H}_{n}^{h}$, which is the desired result. □

Corollary 3.2
Algorithm MPM conserves exactly the total material-point linear momentum and the total material-point angular momentum. The total material-point energy is unconditionally dissipated,

$$\mathsf{H}_{n+1}^{\mathrm{pt}} = \mathsf{H}_{n}^{\mathrm{pt}} - \sum_{\mathrm{pt}=1}^{N_{\mathrm{pt}}} \Delta\mathscr{D}^{\mathrm{int}} \cdot \Omega_0^{\mathrm{pt}} \leqslant \mathsf{H}_{n}^{\mathrm{pt}} \tag{97}$$

Proof
See Reference [5], where it is shown that MPM with a consistent mass matrix inherits the conservation properties of the grid solution. □

4. NUMERICAL SIMULATIONS

The goal of this section is to present some relatively simple numerical simulations which demonstrate the conservation properties of Algorithm MPM. All numerical simulations in this work use a non-linear quasi-Newton root finding algorithm coupled with a matrix-free iterative GMRES linear equation solving algorithm. These are provided by the computational library PETSc [51–53].

4.1. Impact of a Taylor bar

The classical Taylor bar problem [54, 55] is considered. This is a commonly simulated problem and is often used as a benchmark for transient dynamic computer codes [56–58]. A copper bar of radius 3.2 mm and length 32.4 mm impacts a rigid, frictionless wall with an initial longitudinal velocity of 0.227 mm/μs. The material is modelled as elastoplastic with an elastic bulk modulus $K = 130.0$ GPa and an elastic shear modulus $G = 43.3$ GPa. The tension yield (flow) stress is $\sigma_Y = 0.4$ GPa and linear hardening is assumed with $H = 0.1$ GPa and $\eta = 0.0$ Pa s. The material has a density of $\rho_0 = 8.93\,\mathrm{g/cm^3}$.

The bar moves within the rectangular domain $[0.0, 7.2] \times [0.0, 32.4]$, meshed by 9×50 elements. A constant time step of $\Delta t = 1.0\,\mu$s is used for the axisymmetric simulation; 80 time steps are performed. The time histories of radial and axial displacement are shown in Figure 2. The time history of energy is shown in Figure 3. Most numerical simulations of this problem are run for only 80 μs, at which time it has been observed that all the initial kinetic energy has been either dissipated or converted to potential energy. The results of this MPM simulation verify that observation. The sequence of deformed particle configurations, coloured by contour values of equivalent plastic strain, are shown in Figure 4.

All the results are consistent with those in References [9, 21, 56–58].

4.2. Colliding cylinders

The second example simulates the collision of two identical cylinders in plane strain. Each cylinder has an initial radius of 1.0. The cylinders are initially located at $\{-1.05, 0.0\}$ and $\{1.05, 0.0\}$, respectively. The left cylinder is given an initial velocity of $\{1.0, -0.1\}$. The right cylinder is initially at rest. The material parameters are $K = 133.3$, $G = 43.3$, $\sigma_Y = 10.0$, $H = 0.01$ and $\eta = 0.0$. The material has a density of $\rho_0 = 8.824$. This same problem is simulated using energy-consistent plasticity and contact algorithms in Reference [59].

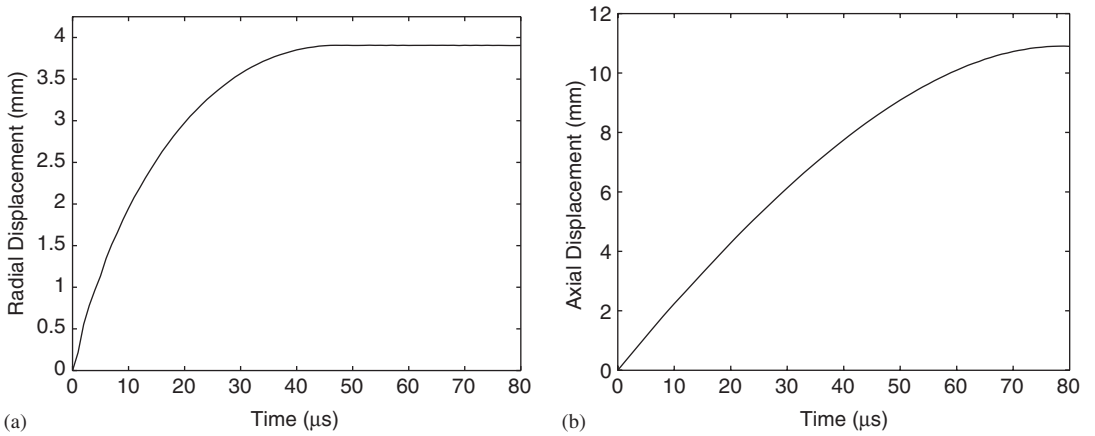

Figure 2. Impact of Taylor bar. Displacement history: (a) maximum radial displacement; and (b) maximum axial displacement.

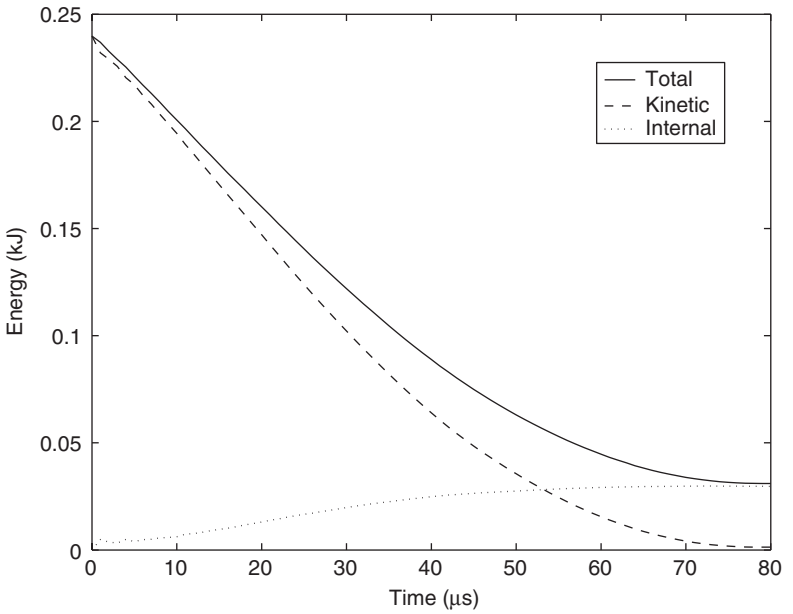

Figure 3. Impact of Taylor bar. Energy evolution.

The cylinders move within the rectangular domain $[-2.20, 2.728] \times [-1.44, 1.20]$, meshed by 28×22 elements. A constant time step of $\Delta t = 0.015$ is used for the simulation; 120 time steps are performed. Figure 5 shows the evolution of energy for the MPM simulation and Figure 6 shows the sequence of the deformed particle configurations, coloured by contours of equivalent plastic strain. The results are in good agreement with Reference [59]. There is no

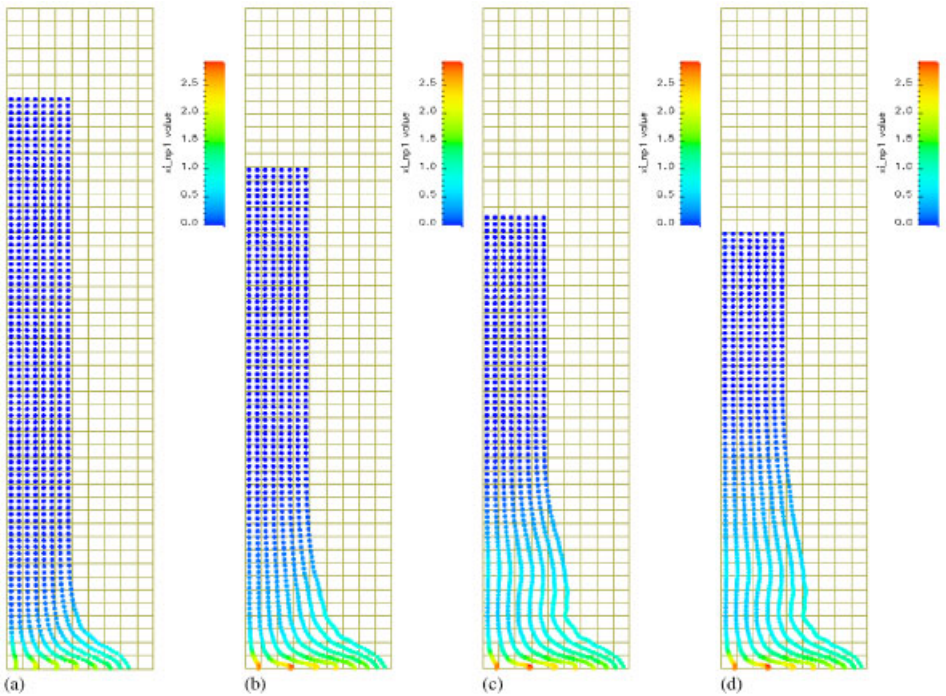

Figure 4. Impact of Taylor bar. Sequence of deformed particle configurations. Contours of equivalent plastic strain time: (a) $t = 20\,\mu s$; (b) $t = 40\,\mu s$; (c) $t = 60\,\mu s$; and (d) $t = 80\,\mu s$.

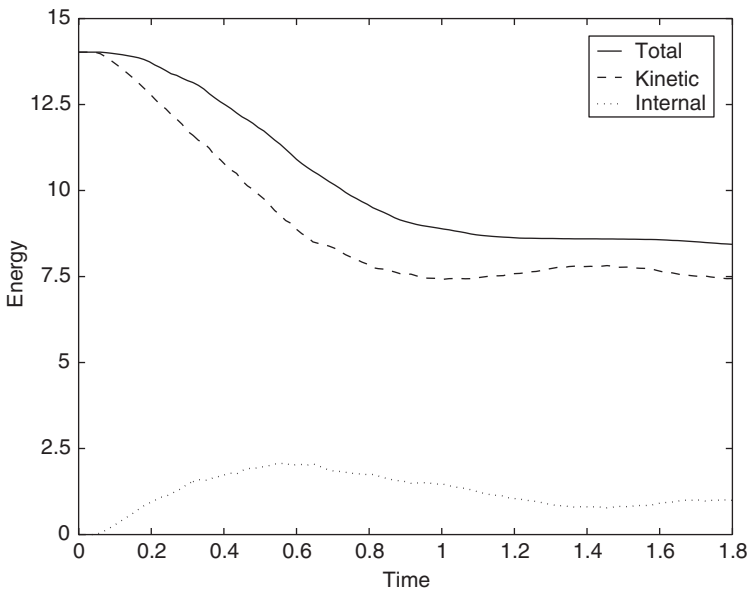

Figure 5. Colliding cylinders. Energy evolution.

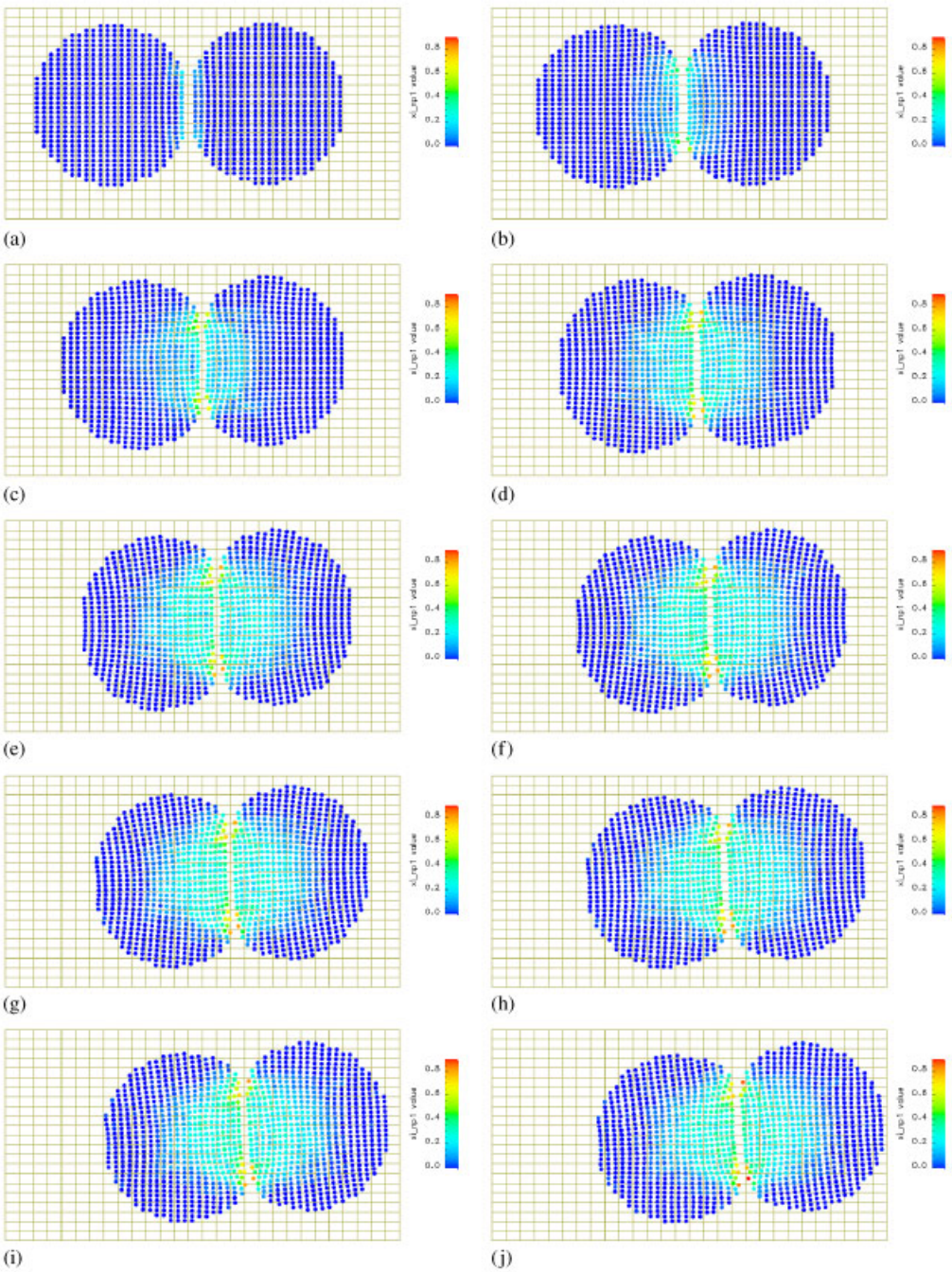

Figure 6. Colliding cylinders. Sequence of deformed particle configurations. Contours of equivalent plastic strain time: (a) $t = 0.18$; (b) $t = 0.36$; (c) $t = 0.54$; (d) $t = 0.72$; (e) $t = 0.90$; (f) $t = 1.08$; (g) $t = 1.26$; (h) $t = 1.44$; (i) $t = 1.62$; and (j) $t = 1.80$.

need to plot the time histories of linear or angular momentum for this example, as both are exactly conserved.

5. CONCLUSIONS

Energy consistency is examined for the MPM algorithm combined with a momentum-conserving and energy-dissipative finite element method for the grid dynamics. When a consistent mass matrix is used the MPM algorithm inherits the conservation properties of the grid solution. In particular, the implicit time integration scheme used for the grid dynamics is designed to reflect the continuum second law of thermodynamics, and conservation of linear and angular momenta. The conserving scheme applies to general hyperelastic-plastic material models and is applied to a multiplicative model of plasticity in the numerical examples. The numerical simulations confirm the theoretical behaviour.

There are some logical extensions of this work. One might consider energy-consistent algorithms for materials exhibiting localized dissipative mechanisms [60, 61]. A promising area is the simulation of Newtonian fluid dynamics, possibly with fluid–structure interaction. The MPM algorithm is more suited to flow calculations than Lagrangian finite element methods. It is also is of interest to examine frictional contact within MPM in the context of energy and momentum-conserving methods. The frictional contact algorithms developed for MPM [62, 63] need modification to ensure that energy is consistently dissipated.

APPENDIX A: ALTERNATIVE IMPLEMENTATIONS OF THE MIXED FORMULATION

Equations (77d)–(77e) are not necessarily the only way to update the element level mixed volume. As alternatives, the following two options are possible:

1. *Incremental multiplicative update*:

$$\sum_{\mathrm{pt}=1}^{N_{\mathrm{pt}}} \delta p^h(\boldsymbol{\varphi}_n^{\mathrm{pt}}) \cdot [\theta^h(\boldsymbol{\varphi}_n^{\mathrm{pt}}) \cdot J_n^{\mathrm{pt}} - J_{n+1}^{\mathrm{pt}}]\, \Omega_0^{\mathrm{pt}} = 0 \tag{A1a}$$

$$\Theta_{n+1}^{\mathrm{pt}} = \theta^h(\boldsymbol{\varphi}_n^{\mathrm{pt}}) \cdot \Theta_n^{\mathrm{pt}} \tag{A1b}$$

   For this update method, an estimate of

$$\sum_{\mathrm{pt}=1}^{N_{\mathrm{pt}}} \delta p^h(\boldsymbol{\varphi}_n^{\mathrm{pt}}) \cdot [\Delta\Theta^{\mathrm{pt}} - \Delta J^{\mathrm{pt}}]\, \Omega_0^{\mathrm{pt}}$$

   cannot be easily computed. Thus, it is not possible to verify the energy conservation properties (or lack thereof) of this update scheme.
2. *Total Lagrangian update*:

$$\sum_{\mathrm{pt}=1}^{N_{\mathrm{pt}}} \delta p^h(\boldsymbol{\varphi}_n^{\mathrm{pt}}) \cdot [\theta_{n+\alpha}^h(\boldsymbol{\varphi}_n^{\mathrm{pt}}) - \det(\mathbf{F}_{n+\alpha}^{\mathrm{pt}})]\Omega_0^{\mathrm{pt}} = 0 \tag{A2a}$$

$$\Theta^{\mathrm{pt}}_{n+\alpha} = \theta^{h}_{n+\alpha}(\boldsymbol{\varphi}^{\mathrm{pt}}_{n}) \tag{A2b}$$

for all $\alpha \in [0, 1]$. In this case there is no need to store Θ at the material points. The average volumes $\{\Theta_n, \Theta_{n+1}\}$ are computed directly. In this case, the values of Θ_n and Θ_{n+1} change during the regrid step(4) of Algorithm MPM since the pressure/volume interpolation changes. The pressure/volume interpolation is grid based, and when particles move to neighbouring elements the mixed volume in those elements changes. Thus, the values of $U(\Theta^{\mathrm{pt}})$ change, and the energy conservation properties of this update scheme are unknown.

Since it is not possible to evaluate the energy conservation properties of these alternatives, the additive update (77d)–(77e) is chosen for this work. However, *all three options are equivalent for a Lagrangian $Q1/P0$ finite element simulation.*

ACKNOWLEDGEMENTS

This material is based upon work supported by the National Science Foundation under Grant No. DMS-0222253.

REFERENCES

1. Sulsky D, Chen Z, Schreyer HL. A particle method for history-dependent materials. *Computer Methods in Applied Mechanics and Engineering* 1994; **118**:179–196.
2. Sulsky D, Schreyer HL. Axisymmetric form of the material point method with applications to upsetting and Taylor impact problems. *Computer Methods in Applied Mechanics and Engineering* 1996; **139**:409–429.
3. Sulsky D, Zhou S-J, Schreyer HL. Application of a particle-in-cell method to solid mechanics. *Computer Physics Communications* 1995; **87**:236–252.
4. Guilkey JE, Weiss JA. Implicit time integration for the material point method: quantitative and algorithmic comparisons with the finite element method. *International Journal for Numerical Methods in Engineering* 2003; **57**(9):1323–1338.
5. Love E, Sulsky DL. An unconditionally stable, energy-momentum consistent implementation of the material-point method. *Technical Report HPC@UNM2004-002*, The Center for High Performance Computing, University of New Mexico, Albuquerque, NM, October 2004 (http://www.hpc.unm.edu).
6. Sulsky D, Kaul A. Implicit dynamics in the material-point method. *Computer Methods in Applied Mechanics and Engineering* 2004; **193**:1137–1170.
7. Moresi L, Dufour F, Muhlhaus HB. A Lagrangian integration point finite element method for large deformation modeling of viscoelastic geomaterials. *Journal of Computational Physics* 2003; **184**(2):476–497.
8. Gonzalez O. Exact energy-momentum conserving algorithms for general models in nonlinear elasticity. *Computer Methods in Applied Mechanics and Engineering* 2000; **190**:1763–1783.
9. Meng XN, Laursen TA. Energy consistent algorithms for dynamic finite deformation plasticity. *Computer Methods in Applied Mechanics and Engineering* 2002; **191**(15–16):1639–1675.
10. Burgess D, Sulsky D, Brackbill JU. Mass matrix formulation of the FLIP particle-in-cell method. *Journal of Computational Physics* 1992; **103**(1):1–15.
11. Antman SS. *Nonlinear Problems of Elasticity*. Applied Mathematical Sciences, vol. 107. Springer: New York, 1995.
12. Ciarlet PG. *Mathematical Elasticity*, *volume I*: *Three-Dimensional Elasticity*. Studies in Mathematics and its Applications, vol. 20. North-Holland: New York, 1988.
13. Gurtin ME. *An Introduction to Continuum Mechanics*. Academic Press: New York, 1981.
14. Marsden JE, Hughes TJR. *Mathematical Foundations of Elasticity*. Dover Publications: New York, 1994.
15. Ogden RW. *Non-Linear Elastic Deformations*. Dover Publications: New York, 1997.
16. Belytschko T, Liu WK, Moran B. *Nonlinear Finite Elements for Continua and Structures*. Wiley: New York, 2000.

17. Simo JC, Taylor RL. Quasi-incompressible finite elasticity in principal stretches. Continuum basis and numerical algorithms. *Computer Methods in Applied Mechanics and Engineering* 1991; **85**:273–310.
18. Simo JC, Taylor RL, Pister KS. Variational and projection methods for the volume constraint in finite deformation elasto-plasticity. *Computer Methods in Applied Mechanics and Engineering* 1985; **51**:177–208.
19. Zienkiewicz OC, Taylor RL. *The Finite Element Method*. Solid Mechanics, (2nd edn). vol. 2. Butterworth-Heinemann: Boston, 2000.
20. Fortin M, Glowinski R. *Augmented Lagrangian Methods*: *Applications to the Numerical Solution of Boundary-Value Problems*. Studies in Mathematics and its Applications, vol. 15. North-Holland: New York, 1983.
21. Simo JC. Algorithms for static and dynamic multiplicative plasticity that preserve the classical return mapping schemes of the infinitesimal theory. *Computer Methods in Applied Mechanics and Engineering* 1992; **99**(1):61–112.
22. Simo JC. Numerical analysis and simulation of plasticity. In *Handbook of Numerical Analysis*, Ciarlet PG, Lions JL (eds), vol. VI. Elsevier: New York, 1998; 183–499.
23. Simo JC, Miehe C. Associative coupled thermoplasticity at finite strains: formulation, numerical analysis and implementation. *Computer Methods in Applied Mechanics and Engineering* 1992; **98**:41–104.
24. Robert JA. Micromechanics of crystals and polycrystals. In *Advances in Applied Mechanics*, Hutchinson JW, Theodore YWu (eds), vol. 23. Academic Press: New York, 1983; 1–115.
25. Lee EH. Elastic-plastic deformations at finite strains. *Journal of Applied Mechanics* (ASME) 1969; **36**:1–6.
26. Xiao H, Chen L-S. Hencky's logarithmic strain and dual stress–strain and strain–stress relations in isotropic finite hyperelasticity. *International Journal of Solids and Structures* 2003; **40**(6):1455–1463.
27. Reese S, Wriggers P. A material model for rubber-like polymers exhibiting plastic deformation: computational aspects and a comparison with experimental results. *Computer Methods in Applied Mechanics and Engineering* 1997; **148**(3–4):279–298.
28. Meschke G, Liu WN. A re-formulation of the exponential algorithm for finite strain plasticity in terms of Cauchy stresses. *Computer Methods in Applied Mechanics and Engineering* 1999; **173**(1–2):167–187.
29. Simo JC, Tarnow N. The discrete energy-momentum method. Conserving algorithms for nonlinear elastodynamics. *Zeitschrift fur Angewandte Mathematik und Physik* (*ZAMP*) 1992; **43**(5):757–792.
30. Cuitino A, Ortiz M. A material-independent method for extending stress update algorithms from small-strain plasticity to finite plasticity with multiplicative kinematics. *Engineering Computations* 1992; **9**:437–451.
31. Weber G, Anand L. Finite deformation constitutive equations and a time integration procedure for isotropic, hyperelastic-viscoplastic solids. *Computer Methods in Applied Mechanics and Engineering* 1990; **79**(2): 173–202.
32. Gonzalez O. Design and analysis of conserving integrators for nonlinear hamiltonian systems with symmetry. *Ph.D. Thesis*, Department of Mechanical Engineering, Stanford University, Stanford, CA, 1996.
33. Armero F, Romero I. On the formulation of high-frequency dissipative time-stepping algorithms for nonlinear dynamics. Part I. Low-order methods for two model problems and nonlinear elastodynamics. *Computer Methods in Applied Mechanics and Engineering* 2001; **190**:2603–2649.
34. Armero F, Romero I. On the formulation of high-frequency dissipative time-stepping algorithms for nonlinear dynamics. Part II. Second-order methods. *Computer Methods in Applied Mechanics and Engineering* 2001; **190**:6783–6824.
35. Papadopoulos P. Lu J. A general framework for the numerical solution of problems in finite elasto-plasticity. *Computer Methods in Applied Mechanics and Engineering* 1998; **159**(1–2):1–18.
36. Reese S, Govindjee S. A theory of finite viscoelasticity and numerical aspects. *International Journal of Solids and Structures* 1998; **35**(26–27):3455–3482.
37. Miehe C. Exponential map algorithm for stress updates in anisotropic multiplicative elastoplasticity for single crystals. *International Journal for Numerical Methods in Engineering* 1996; **39**(19):3367–3390.
38. Steinmann P, Stein E. On the numerical treatment and analysis of finite deformation ductile single crystal plasticity. *Computer Methods in Applied Mechanics and Engineering* 1996; **129**(3):235–254.
39. Feng L, Zhang KS, Zhang G, Yu HD. Anisotropic damage model under continuum slip crystal plasticity theory for single crystals. *International Journal of Solids and Structures* 2002; **39**(20):5279–5293.
40. Simo JC. On a fully three-dimensional finite-strain viscoelastic damage model: formulation and computational aspects. *Computer Methods in Applied Mechanics and Engineering* 1987; **60**:153–173.
41. Wieckowski Z. The material point method in large strain engineering problems. *Computer Methods in Applied Mechanics and Engineering* 2004; **193**(39–41):4417–4438.
42. Brezzi F, Fortin M. *Mixed and Hybrid Finite Element Methods*. Springer Series in Computational Mathematics, vol. 15. Springer: New York, 1991.

43. Ern A, Guermond J-L. *Theory and Practice of Finite Elements*. Applied Mathematical Sciences, vol. 159. Springer: New York, 2004.
44. Oden JT, Kikuchi N, Song YJ. Penalty-finite element methods for the analysis of Stokesian flows. *Computer Methods in Applied Mechanics and Engineering* 1982; **31**(3):297–329.
45. Brenner SC, Scott LR. *The Mathematical Theory of Finite Element Methods*. Texts in Applied Mathematics, vol. 15. Springer: New York, 1994.
46. Malkus DS, Olsen ET. Obtaining error estimates for optimally constrained incompressible finite elements. *Computer Methods in Applied Mechanics and Engineering* 1984; **45**(1–3):331–353.
47. Carey GF, Oden JT. *Finite Elements*, *volume II*: *A Second Course*. Prentice-Hall: Englewood Cliffs, NJ, 1983.
48. Hughes TJR, Liu WK, Brooks A. Finite element analysis of incompressible viscous flows by the penalty function formulation. *Journal of Computational Physics* 1979; **30**(1):1–60.
49. Sani RL, Gresho PM, Lee RL, Griffiths DF. The cause and cure of the spurious pressures generated by certain FEM solutions of the incompressible Navier–Stokes equations I. *International Journal for Numerical Methods in Fluids* 1981; **1**(1):17–43.
50. Sani RL, Gresho PM, Lee RL, Griffiths DF, Engelman M. The cause and cure of the spurious pressures generated by certain FEM solutions of the incompressible Navier–Stokes equations. II. *International Journal for Numerical Methods in Fluids* 1981; **1**(2):171–204.
51. Balay S, Buschelman K, Eijkhout V, Gropp WD, Kaushik D, Knepley MG, McInnes LC, Smith BF, Zhang H. PETSc users manual. *Technical Report ANL-95/11—Revision 2.1.5*, Argonne National Laboratory, 2004.
52. Balay S, Buschelman K, Gropp WD, Kaushik D, Knepley MG, McInnes LC, Smith BF, Zhang H. PETSc Web page, 2001. http://www.mcs.anl.gov/petsc
53. Balay S, Eijkhout V, Gropp WD, McInnes LC, Smith BF. Efficient management of parallelism in object oriented numerical software libraries. *Modern Software Tools in Scientific Computing*. Birkhäuser: Basel, 1997; 163–202.
54. Taylor G. The use of flat-ended projectiles for determining dynamic yield stress. I. Theoretical considerations. *Proceedings of the Royal Society of London*, *Series A*, *Mathematical and Physical Sciences* 1948; **194**(1038):289–299.
55. Wilkins ML, Guinan MW. Impact of cylinders on a rigid boundary. *Journal of Applied Physics* 1973; **44**(3):1200–1206.
56. Engelmann BE, Hallquist JO. *Nike2D User Manual*. Lawrence Livermore National Laboratory: Livermore, CA, 1991.
57. Gadala MS. Recent trends in ALE formulation and its applications in solid mechanics. *Computer Methods in Applied Mechanics and Engineering* 2004; **193**(39–41):4247–4275.
58. Maker BN, Ferencz RN, Hallquist JO. *Nike3D User Manual*. Lawrence Livermore National Laboratory: Livermore, CA, 1995.
59. Meng XN, Laursen TA. On energy consistency of large deformation plasticity models, with application to the design of unconditionally stable time integrators. *Finite Elements in Analysis and Design* 2002; **38**: 949–963.
60. Armero F. Large-scale modeling of localized dissipative mechanisms in a local continuum: applications to the numerical simulation of strain localization in rate-dependent inelastic solids. *Mechanics of Cohesive-Frictional Materials* 1999; **4**(2):101–131.
61. Armero F, Garikipati K. An analysis of strong discontinuities in multiplicative finite strain plasticity and their relation with the numerical simulation of strain localization in solids. *International Journal of Solids and Structures* 1996; **33**(20–22):2863–2885.
62. Bardenhagen S, Brackbill J, Sulsky D. The material-point method for granular materials. *Computer Methods in Applied Mechanics and Engineering* 2000; **187**:529–541.
63. Cummins SJ, Brackbill JU. An implicit particle-in-cell method for granular materials. *Journal of Computational Physics* 2002; **180**:506–548.

